Article

Cell Reports

Regulation of Breast Cancer-Induced Osteoclastogenesis by MacroH2A1.2 Involving EZH2-Mediated H3K27me3

Graphical Abstract

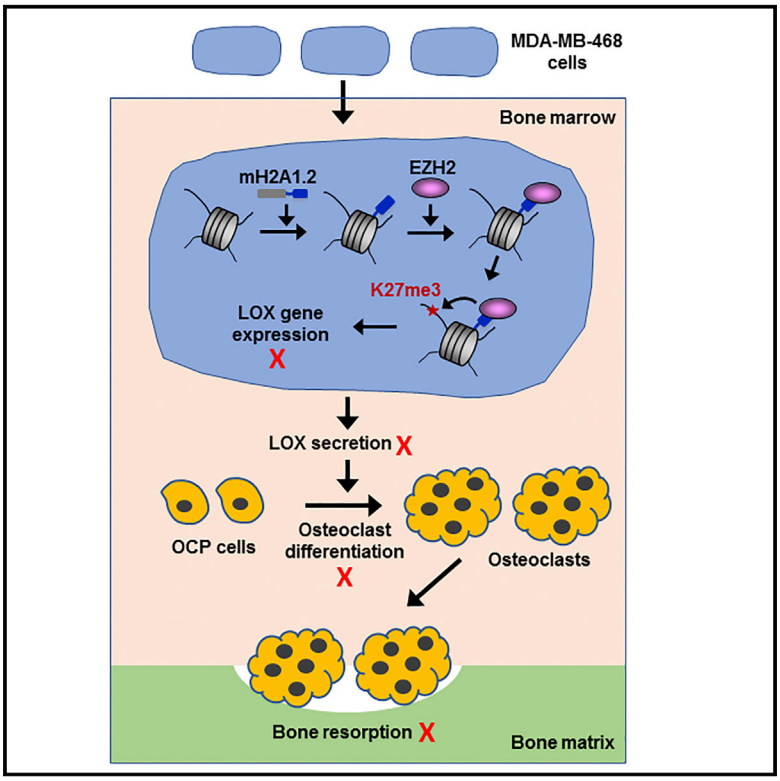

Authors

Jinman Kim, Yonghwan Shin, Sunyoung Lee, ..., Jungmin Koh, Daewon Jeong, Woojin An

Correspondence

woojinan@usc.edu

In Brief

Kim et al. demonstrate that mH2A1.2 attenuates breast cancer-induced osteoclastogenesis by maintaining the LOX gene in an inactive state. Mechanistically, mH2A1.2 recruits EZH2 to induce H3K27me3 and create a repressive barrier to LOX transcription.

Highlights

- mH2A1.2 inhibits the expression of genes encoding osteoclastogenic soluble factors
- LOX is necessary for mH2A1.2 to attenuate breast cancer-induced osteoclastogenesis
- LOX targets the c-Src signal transduction pathway
- mH2A1.2 cooperates with EZH2 to inhibit LOX expression and osteoclastogenesis

Data and Software Availability

GSE107570

Kim et al., 2018, Cell Reports *24*, 224–237
July 3, 2018
https://doi.org/10.1016/j.celrep.2018.06.020

CellPress

OPEN ACCESS
CellPress

Cell Reports
Article

Regulation of Breast Cancer-Induced Osteoclastogenesis by MacroH2A1.2 Involving EZH2-Mediated H3K27me3

Jinman Kim,[1] Yonghwan Shin,[1] Sunyoung Lee,[1] Miyeong Kim,[2] Vasu Punj,[3] Jason F. Lu,[1] Hongin Shin,[4] Kyunghwan Kim,[1,5] Tobias S. Ulmer,[6] Jungmin Koh,[7] Daewon Jeong,[2] and Woojin An[1,8,*]

[1]Department of Biochemistry and Molecular Medicine, Norris Comprehensive Cancer Center, University of Southern California, Los Angeles, CA 90033, USA
[2]Department of Microbiology, College of Medicine, Yeungnam University, Daegu 705-717, Republic of Korea
[3]Department of Medicine, Norris Comprehensive Cancer Center, University of Southern California, Los Angeles, CA 90033, USA
[4]Department of Oral Pathology, School of Dentistry, Kyungpook National University, Daegu 700-412, Republic of Korea
[5]Department of Biology, College of Natural Sciences, Chungbuk National University, Cheongju 361-763, Republic of Korea
[6]Department of Biochemistry and Molecular Medicine, Zilkha Neurogenetic Institute, University of Southern California, Los Angeles, CA 90033, USA
[7]Division of Endocrinology and Metabolism, Asan Medical Center, University of Ulsan College of Medicine, Seoul 138-736, Republic of Korea
[8]Lead Contact
*Correspondence: woojinan@usc.edu
https://doi.org/10.1016/j.celrep.2018.06.020

SUMMARY

Breast cancer cells relocate to bone and activate osteoclast-induced bone resorption. Soluble factors secreted by breast cancer cells trigger a cascade of events that stimulate osteoclast differentiation in the bone microenvironment. MacroH2A is a unique histone variant with a C-terminal non-histone domain and plays a crucial role in modulating chromatin organization and gene transcription. Here, we show that macroH2A1.2, one of the macroH2A isoforms, has an intrinsic ability to inhibit breast cancer-derived osteoclastogenesis. This repressive effect requires macroH2A1.2-dependent attenuation of expression and secretion of lysyl oxidase (LOX) in breast cancer cells. Furthermore, our mechanistic studies reveal that macroH2A1.2 physically and functionally interacts with the histone methyltransferase EZH2 and elevates H3K27me3 levels to keep LOX gene in a repressed state. Collectively, this study unravels a role for macroH2A1.2 in regulating osteoclastogenic potential of breast cancer cells, suggesting possibilities for developing therapeutic tools to treat osteolytic bone destruction.

INTRODUCTION

Histone variants are non-allelic isoforms of canonical histones and play important roles in mediating dynamic changes in chromatin structure and gene transcription (Henikoff and Smith, 2015; Maze et al., 2014). One such histone variant is macroH2A (mH2A). mH2A has a tripartite structure consisting of an N-terminal histone-fold, an unstructured linker domain, and a unique C-terminal macrodomain (Pehrson and Fried, 1992). In vertebrates, there are two mH2A isoforms, mH2A1 and mH2A2, which are encoded by separate genes. Two closely related subtypes of mH2A1, mH2A1.1 and mH2A1.2, are produced by alternative splicing in the macrodomain. mH2A is widely enriched in the inactive X chromosome and is nonrandomly distributed in specific chromosomal regions such as pseudoautosomal region and scaffold attachment region (Henikoff and Smith, 2015; Turner et al., 2001). This accumulation of mH2A has been proposed to contribute to long-term maintenance of gene silencing in these genomic regions. Beside its role in X chromosome inactivation, mH2A can also modulate specific gene transcription both negatively and positively (Dell'Orso et al., 2016; Gamble et al., 2010; Kapoor et al., 2010; Kim et al., 2013). These properties of mH2A may be generated through physical and functional interactions with gene specific regulators, as supported by previous studies showing that HDAC1/2, PARP1, and Pbx1 are recruited by mH2A1 and necessary for establishing distinct transcription states (Buschbeck et al., 2009; Chakravarthy et al., 2005; Chen et al., 2014; Dell'Orso et al., 2016; Kim et al., 2013).

Bone remodeling is a tightly regulated process responsible for bone resorption and formation through a series of steps that depend on the coordinated action of two cell lineages, osteoclasts and osteoblasts (Karsenty et al., 2009). Osteoclasts are large multinucleated hematopoietic cells responsible for bone resorption, whereas osteoblasts are bone-forming cells with a single nucleus (Raggatt and Partridge, 2010). Osteoclast precursor (OCP) cells are progressively differentiated into mature osteoclasts by fusion over a period of several days. The interaction of receptor activator of nuclear factor κB (NF-κB) ligand (RANKL), which is expressed as a membrane-bound protein in osteoblasts, with RANK on OCP cell membrane induces the initial expression of master transcription factors such as NF-κB, c-Fos, and NFATc1 (Karsenty et al., 2009; Raggatt and Partridge, 2010). These osteoclastogenic factors, then, trigger major signaling pathways to turn on multiple downstream genes encoding key determinants of osteoclast differentiation (Boyle et al., 2003; Teitelbaum and Ross, 2003). It is becoming evident that the deregulation of osteoclastogenic activity under certain

pathological conditions leads to abnormal bone remodeling and contributes to the pathogenesis of bone disorders such as osteoporosis, rheumatoid arthritis, and bone metastases (Zaidi, 2007).

Breast cancer is the most common cancer in women and frequently metastasizes to bone and disrupts the normal bone remodeling process (Weilbaecher et al., 2011). While breast cancer bone metastases can be classified as osteolytic or osteoblastic, osteolytic bony changes are most frequently observed during the pathogenic processes (Weilbaecher et al., 2011). Breast cancer cells residing in bone express and secrete a plethora of osteolytic factors that stimulate osteoclast differentiation and maturation. (Kang et al., 2003; Weilbaecher et al., 2011). This unbalanced generation of osteoclasts by breast cancer-secreted factors leads to a massive bone resorption and causes osteoclast-mediated bone destruction. In turn, this destruction causes the release of bone matrix-stored growth factors, which act on cancer cells to produce osteoclastogenic factors and fuel a feed-forward vicious cycle in the bone. Thus, the identification of secreted factors capable of promoting osteoclast formation, activation, and survival is crucial in preventing and reducing the osteolytic bone metastases of breast cancer (Clézardin, 2011; Yin et al., 2005).

Because genes encoding secreted factors are stored in the nucleus by chromatinization, a fundamental mechanism underlying breast cancer-induced osteoclastogenesis might be regulated through chromatin-dependent pathways. In fact, previous studies including ours identified some of histone modifications as possible mechanisms underlying epigenetic regulation of osteoclastogenic transcription programs (Kim et al., 2016b; Zhang et al., 2015). Despite these advances, however, nothing is currently known about the effects of histone variants on the process of osteoclast differentiation. Here, we show that mH2A1.2 inhibits the expression and secretion of soluble factors influencing osteoclast differentiation and function in the process of breast cancer bone metastases. We then demonstrate that EZH2 histone methyltransferase is required for mH2A1.2-dependent generation of inactive chromatin domain and suppression of osteoclastogenic genes in breast cancer cells.

RESULTS

mH2A1.2 Suppresses Osteoclastogenic Potential of Breast Cancer Cell-Secreted Factors

As an initial step in our investigation, we set up an assay system to determine the effects of breast cancer cell conditioned media (CMs) on osteoclast differentiation (Figure 1A). The suitability of this assay system was confirmed by the finding that osteoclast precursor (OCP) cells are synchronously differentiated into TRAP-positive multinuclear osteoclasts in α-minimal essential medium (α-MEM) following treatment with M-CSF, RANKL and CMs (Figure 1B). Under these conditions, higher numbers of mature osteoclast were generated, when OCP cells were cultured for 6 days in a 1:1 mixture of α-MEM and CMs prepared from moderately metastatic MDA-MB-468 breast cancer cells (Figure 1B). To analyze possible roles played by histone variants in regulating CM-induced osteoclastogenesis, analogous assays were carried out using CMs from MDA-MB-468 cells infected with lentiviruses encoding a short hairpin RNA (shRNA) against each of histone variants. The fact that shRNA-mediated downregulation of one histone variant did not affect the expression of other histone variants made it possible to functionally evaluate each of the histone variants (Figure S1A). When the effects of depletion of endogenous H2AX, H2A.Z, mH2A2, H2ABbd, H3.3, or CENP-A in MDA-MB-468 cells were examined in differentiation assays with MDA-MB-468 CMs, undetectable or only minor changes were observed in the formation of mature osteoclasts (Figure 1E). On the other hand, the treatment of OCP cells with CMs from mH2A1-depleted MDA-MB-468 cells significantly increased the number of differentiated osteoclasts (Figure 1E).

Because mH2A1.1 and mH2A1.2 isoforms were co-depleted by transfecting OCP cells with mH2A1 shRNA in our assays, we tried to individually knockdown them. However, the high degree of sequence homology between mH2A1.1 and mH2A1.2 mRNAs made it difficult. Hence, we took the alternative approach of transfecting RNAi-resistant, FLAG-tagged mH2A1.1, or mH2A1.2 in mH2A1-depleted MDA-MB-468 cells and determining if there is a change in osteoclastogenic effects of CMs (Figure S1B). As indicated by TRAP staining, the ectopic expression of mH2A1.2 in mH2A1-depleted cells significantly reduced the osteoclastogenic property of CMs (Figure 1C). However, ectopic mH2A1.1 was unable to substitute for the anti-osteoclastogenic function of mH2A1.2 within the scope of this analysis (Figure 1C). Consistent with these data, treatment of OCP cells with CMs from mH2A1-depleted cells expressing FLAG-tagged mH2A1.2, but not mH2A1.1, blocked the induction of NFATc1 and its downstream target genes ATP6V0D2 and cathepsin K (Figure 1D). We also found that mH2A1.2 overexpression in MDA-MB-468 cells inhibits CM-induced osteoclast formation by ~70% (Figures S1C and S1D). Expectedly, however, ectopic expression of mH2A1.1 in MDA-MB-468 cells resulted in no detectable effects on CM-induced osteoclastogenesis (Figures S1C and S1D). These observations are in consonance with our knockdown experiment data and underscore the notion that mH2A1.2 has repressive effects on CM osteoclastogenic activity.

Beside CMs from moderately metastatic MDA-MB-468 cells, we also examined the osteoclastogenic effects of CMs from nonmetastatic MCF-7 and highly metastatic MDA-MB-231 breast cancer cells as well as MCF-10-2A normal breast cells. As confirmed by western blot, highly metastatic MDA-MB-231 cancer cells expressed less mH2A1 than moderately metastatic MDA-MB-468 and nonmetastatic MCF-7 cancer cells (Figure S2A). In contrast, mH2A1 expression level was much higher in MCF-10-2A normal breast cells compared with three other breast cancer cell lines (Figure S2A). When CMs from these cell lines were analyzed in osteoclast differentiation assays, MDA-MB-231 CMs were far more osteoclastogenic, generating 3 times higher numbers of $TRAP^+$ mature osteoclasts compared with MDA-MB-468 CMs (Figure S2B). Conversely, addition of MCF-7 and MCF-10-2A CMs to OCP cell culture failed to generate multinucleated cells with phenotypic features of osteoclasts (Figure S2B).

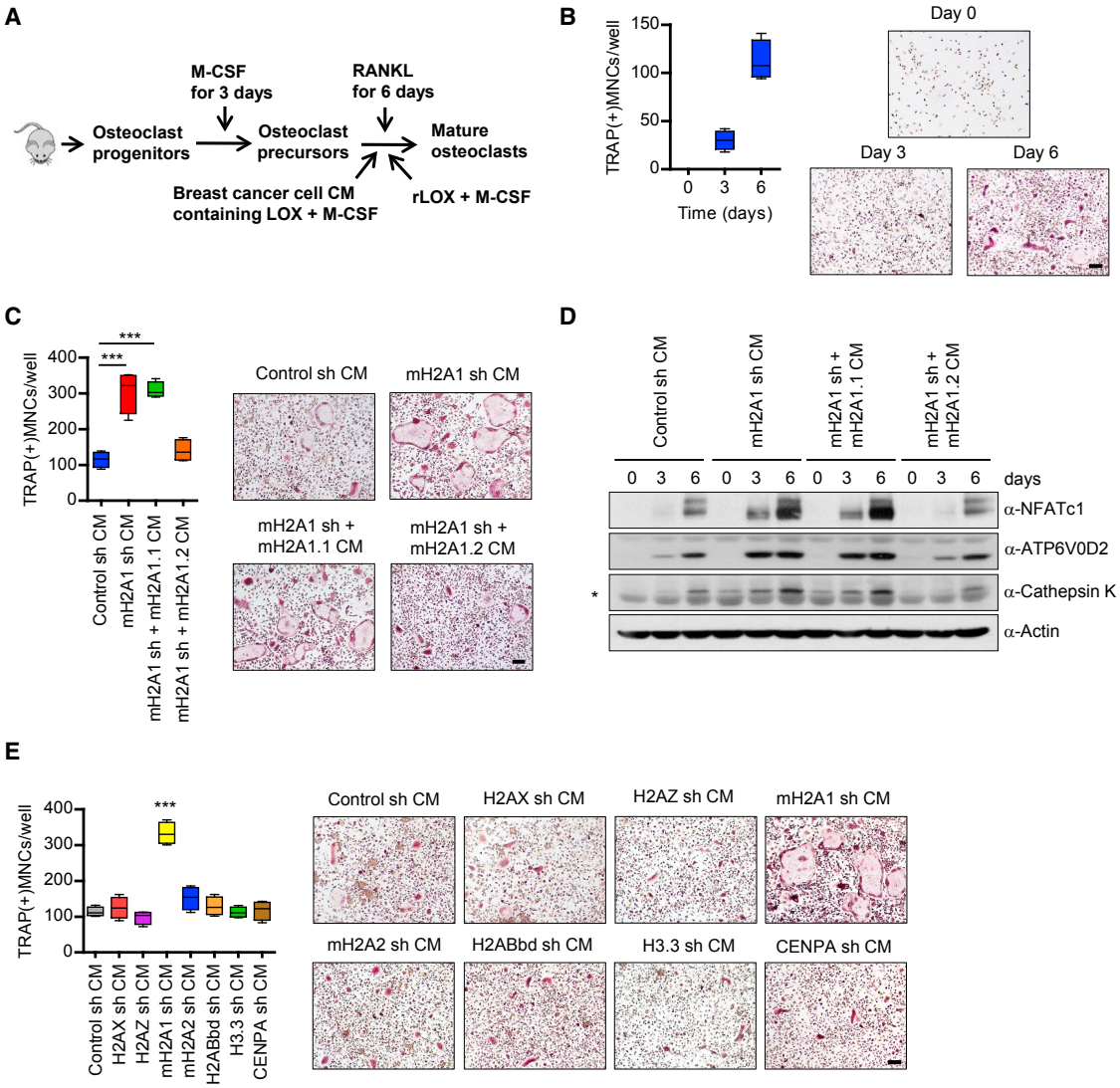

Figure 1. Inhibition of Osteoclastogenic Activity of Breast Cancer Cell CMs by mH2A1.2

(A) Shown are the steps for analysis of osteoclastogenic properties of breast cancer cell-derived conditioned media (CMs) and recombinant LOX (rLOX).

(B) OCP cells were incubated with RANKL and MDA-MB-468 CMs for 0, 3, or 6 days, fixed, stained for TRAP, and photographed under a light microscope (10×) (right). Representative images of osteoclasts are shown (scale bar, 100 μm). TRAP positive multinucleated cells (TRAP(+)MNCs) containing three or more nuclei and a full actin ring were counted as osteoclasts (left). Scale bar, 100 μm.

(C) CMs were prepared from mH2A1-depleted MDA-MB-468 cells expressing exogenous shRNA-resistant mH2A1.1 or mH2A1.2 and analyzed for osteoclastogenic activity as in (B). Scale bar, 100 μm. Error bars are the means ± SD (n = 4) of three independent experiments; ***p < 0.001 (ANOVA analysis).

(D) Cell lysates were collected from OCP cells after treating with MDA-MB-468 CMs for the indicated time periods and analyzed for the expression of three osteoclast markers (NFATc1, ATP6V0D2, and cathepsin K) by western blot. β-Actin was used as a loading control. Non-specific band was marked by asterisk.

(E) OCP cells were cultured with CMs collected from MDA-MB-468 breast cancer cells depleted of the indicated histone variants. At the end of day 6, OCP-induced cells were stained for TRAP (right) to measure osteoclast differentiation (left). Error bars represent the means ± SD (n = 4); ***p < 0.001 versus Control sh CM (ANOVA analysis).

mH2A1.2 Inactivates the Genes Encoding Secreted Osteoclastogenic Factors in Breast Cancer Cells

The data presented above strongly suggest a potential role of mH2A1.2 in the regulation of osteoclastogenic activity of CMs from breast cancer cells, particularly moderately metastatic cells. To assess whether this reflects transcriptional regulation of genes encoding secreted factors, we examined the transcriptome of secretory protein genes by comparing the mRNA profiles of mock-depleted and mH2A1-depleted MDA-MB-468 breast cancer cells. Recent technological advances provide unique opportunities to globally identify potential candidate genes whose products could regulate the progression of bone metastasis. Although such genome-wide studies produced several databases summarizing known or predicted secreted

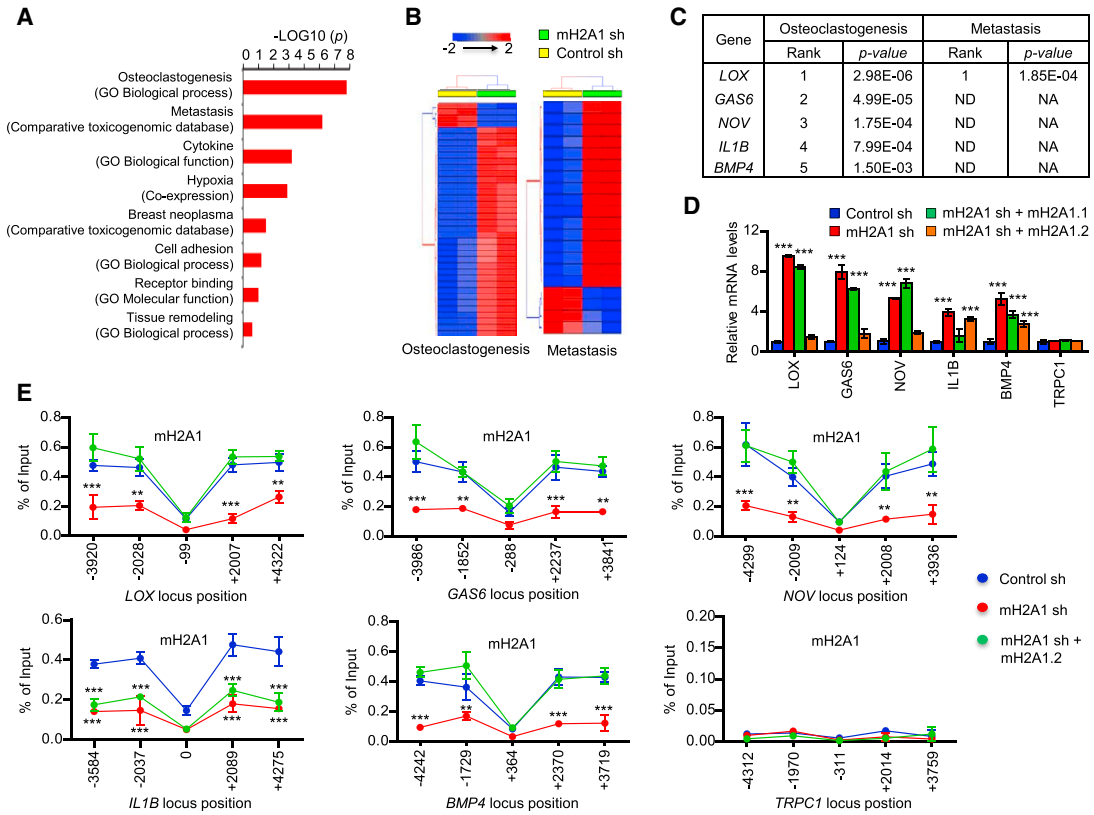

Gene	Osteoclastogenesis		Metastasis	
	Rank	*p-value*	Rank	*p-value*
LOX	1	2.98E-06	1	1.85E-04
GAS6	2	4.99E-05	ND	NA
NOV	3	1.75E-04	ND	NA
IL1B	4	7.99E-04	ND	NA
BMP4	5	1.50E-03	ND	NA

Figure 2. Identification of mH2A1.2 Target Genes in Breast Cancer Cells

(A) Pathway analysis of breast cancer secretome identified the enrichment of pathways related to breast cancer associated bone metastasis and osteoclastogenesis in 3,948 secretome genes. A ranked p value was computed for each pathway based on hypergeometric distribution along with Benjamini Hochberg correction ($p < 0.05$). Datasets used to extract the pathway terms are indicated in parentheses. The genes identified in each pathway are listed in Table S3.

(B) A two-way hierarchical clustering of two representative pathways—osteoclast differentiation and metastasis—showing distinct signature expression profile in mH2A1 sh knockdown and wild-type MDA-MB-486 cells. Euclidean distance and Average linkage were used for clustering.

(C) Prioritization of candidate genes in two important pathways differentially regulated in control and mH2A1-depleted MDA-MB-486 cells. Genes are ranked in the order of their functional statistical significance in a particular pathway. Top five ranked genes in osteoclast differentiation pathway and their corresponding rank in metastatic pathway are shown.

(D) qRT-PCR was performed to quantify relative mRNA levels of the top five genes using primers listed in Table S4. Error bars denote the SD from triplicate reactions by real-time PCR; ***$p < 0.001$ versus Control sh (ANOVA analysis).

(E) ChIP assays were performed at five different regions of the five mH2A1.2-repressed and one control genes using mH2A1 antibody and primers listed in Table S4. Error bars denote the means ± SD obtained from triplicate real-time PCR reactions; **$p < 0.01$, ***$p < 0.001$ versus Control sh (ANOVA analysis).

factors, those databases are incomplete or in inconsistent formats that use different types of protein and gene identifiers. To overcome these limitations, we collected public databases as well as published papers providing lists of secreted proteins, transmembrane proteins, and signal peptides, and constructed a breast cancer secretome through *in silico* approaches. As detailed in the Experimental Procedures, we used a bioinformatics approach and curated secretory proteins in GRCh37 genome in each database (Table S2). In total, 3,948 genes were selected for quantitative comparison of mRNA levels in mock-depleted control and mH2A1-depleted MDA-MB-468 cells.

In conventional microarray data analysis, genes exhibiting significantly different expression levels between two phenotypes are selected and analyzed for biological functions. However, it is becoming increasingly clear that smaller but coordinated expression changes in a set of genes involved in a particular biological process may dictate the biological pathway associated with a specific phenotype (Bild et al., 2006). Therefore, we decided to analyze microarray data at the level of pathways without including any pre-determined fold change filtering in our analysis. We found that pathways involved in metastasis as well as the crosstalk between bone cells and cancer cells are enriched in mH2A1-depleted MDA-MB-468 cells (Figure 2A; Table S3; false discovery rate [FDR] $p < 0.05$). In supervised two-way hierarchical clustering of gene expression data, two representative pathways, osteoclastogenesis and metastasis, showed a distinct signature profile of mH2A1-depleted cells over control cells, suggesting that mH2A1 plays a critical role in governing the expression of osteoclastogenic and metastatic genes in MDA-MB-468 cells (Figure 2B). When we further focus our analysis on osteoclastogenesis and metastasis pathways, lysyl oxidase (LOX) gene was ranked at the top in these categories

(Figure 2C). The datasets resulting from microarray-based secretome analysis were further confirmed by qRT-PCR (Figure 2D). As we made use of mH2A1-depleted MDA-MB-468 cells to generate microarray data, mH2A1.1 or mH2A1.2 was again transfected into these cells to distinguish mH2A1.1-specific versus mH2A1.2-specific target genes. Expression of ectopic mH2A1.2 inhibited three out of five genes encoding secreted bone remodeling factors that were most highly expressed in mH2A1-depleted MDA-MB-468 cells (Figure 2D). Among the two remaining genes, one gene was inactivated by ectopic mH2A1.1, while the other gene was slightly affected by both ectopic mH2A1.1 and mH2A1.2 (Figure 2D).

Whereas the above results suggested a role for mH2A1.2 in suppressing osteoclastogenic and metastasis-promoting genes, we could not discriminate between direct and indirect effects of mH2A1.2 knockdown on target genes in this analysis. We therefore used chromatin immunoprecipitation (ChIP) assays to investigate whether mH2A1.2 localizes along the potential target genes. Because ChIP-grade mH2A1.2-specific antibody is not available, a mH2A1 antibody detecting both mH2A1.1 and mH2A1.2 was used in these experiments. DNA obtained from immunoprecipitation with this antibody was subjected to real-time PCR using primers targeting five different regions of the target genes. Primer pairs amplifying regions ~2 and 4 kb upstream or downstream of the transcription start site (TSS) revealed a substantial enrichment of mH2A1 (Figure 2E). As a control, mH2A1 was not detected at *TRPC1* gene and failed to show any changes in response to mH2A1 knockdown. ChIP analysis using H3 antibody showed little fluctuation in signals along the five different regions of the target genes, indicating similar levels of nucleosome occupancy at those regions (Figure S2C). When ChIP experiments were performed in mH2A1-depleted MDA-MB-468 cells, almost complete loss of mH2A1 ChIP signals was detected at the five target genes (Figure 2E). Similar analysis after expressing ectopic mH2A1.2 in mH2A1-depleted cells failed to show the recovery of ChIP signals at *IL1B* gene, results indicative of the incapability of mH2A1.2 to localize at this gene (Figure 2E). Expectedly, however, rescue expression of mH2A1.2 largely overrides the ChIP signal defects caused by mH2A1 knockdown at *LOX*, *GAS6*, *NOV*, and *BMP4* genes (Figure 2E), strongly suggesting that mH2A1.2 is responsible for mH2A1 ChIP signals observed in these four target genes.

LOX Is a mH2A1.2 Target Gene and Is Necessary for mH2A1.2 Function

A noteworthy observation emerged from our secretome-based microarray data analysis was that mH2A1 depletion in MDA-MB-468 breast cancer cells most significantly activated the expression of LOX. Because LOX is known to facilitate the dissemination of cancer cells in the bone marrow, formation of mature osteoclasts, and generation of osteolytic lesions (Cox et al., 2015; Reynaud et al., 2017; Tsukasaki et al., 2017), we decided to examine whether LOX is responsible for the major osteoclastogenic activity of CMs and behaves as a primary downstream target for mH2A1.2. Accordingly, we transfected MDA-MB-468 cells with specific shRNAs against LOX and mH2A1 alone or together (Figure 3A). Upon stable knockdown of LOX, LOX activity in CMs was drastically reduced as shown by *in vitro* oxidase assays (Figure 3B). LOX gene expression was fully activated under mH2A1 knockdown condition (Figure 3A). When OCP cells were treated with CMs from MDA-MB-468 cells depleted of LOX, the effects of CMs on RANKL-induced osteoclast differentiation and osteoclast-specific gene expression were significantly attenuated (Figure 3C). Furthermore, ectopic expression of LOX wild-type, but not LOX oxidase-dead K320A mutant (Erler et al., 2009), in MDA-MB-468 cells substantially rescued the osteoclastogenic potential and LOX activity of CMs (Figures 3D and S3). In accordance with these findings, our western blot analysis showed that osteoclast differentiation marker genes (NFATc1, ATP6V0D2, and cathepsin K) were more highly expressed in control CM-treated OCP cells compared to LOX-depleted OCP cells (Figure 3E). These results argue against the possibility that the observed effects of LOX shRNA are generated by off-target effects and indicate that osteoclastogenic function of LOX is indeed accurately established in our assays. Importantly, knockdown of mH2A1 in LOX-deficient MDA-MB-468 cells was unable to augment osteoclastogenic potential of CMs (Figure 3C), reinforcing the conclusion that anti-osteoclastogenic function of mH2A1.2 is dependent on its inhibitory activity against LOX expression. Further support for our conclusion came from the observed enhancement of osteoclastogenesis after treatment with CMs from LOX-transfected MCF-7 cells that have low levels of endogenous LOX (Figures S2 and S3).

Given that breast cancer-mediated osteoclastogenesis involves several distinct steps, we also investigated the impact of altering LOX levels on OCP cell migration and MDA-MB-468 cell invasion. It was apparent in these experiments that knockdown and ectopic expression of LOX reduced and restored, respectively, the capacity of CMs to stimulate OCP cell migration (Figures S3E and S3F, left). Similar results were obtained from invasion assays using MDA-MB-468 cells (Figures S3E and S3F, right). Because knocking down mH2A1 in LOX-depleted MDA-MB468 cells failed to generate stimulatory effects in our assays (Figure S3E), these findings indicate that mH2A1.2 constitutes a repressive barrier to OCP and MDA-MB-468 cells in a LOX-dependent fashion.

For the purpose of further validating the stimulatory role of LOX in the osteoclastogenesis process, OCP cells were treated with recombinant LOX (rLOX) in the presence of M-CSF and RANKL. When incubated with rLOX wild-type (rLOX wt) for 6 days, OCP cells were differentiated into osteoclasts and expressed osteoclast marker genes (NFATc1, ATP6V0D2, and cathepsin K) at much higher levels compared with mock-treated control cells (Figures 3F and 3G). In contrast, however, no changes in osteoclast differentiation and marker gene expression were detected in OCP cells treated with rLOX oxidase-dead mutant (rLOX mt) (Figures 3F and 3G). In agreement with the knockdown data (Figures S3E and S3F), treatment with rLOX also potentiates transwell movements of OCP cells, again linking LOX to OCP cell migration and MDA-MB-468 invasion (Figure S3G).

LOX Is a Positive Regulator of Osteoclast Differentiation and Bone Resorption

As an extension of the above-described study, we plated osteoclasts on dentin slices and evaluated the effects of rLOX

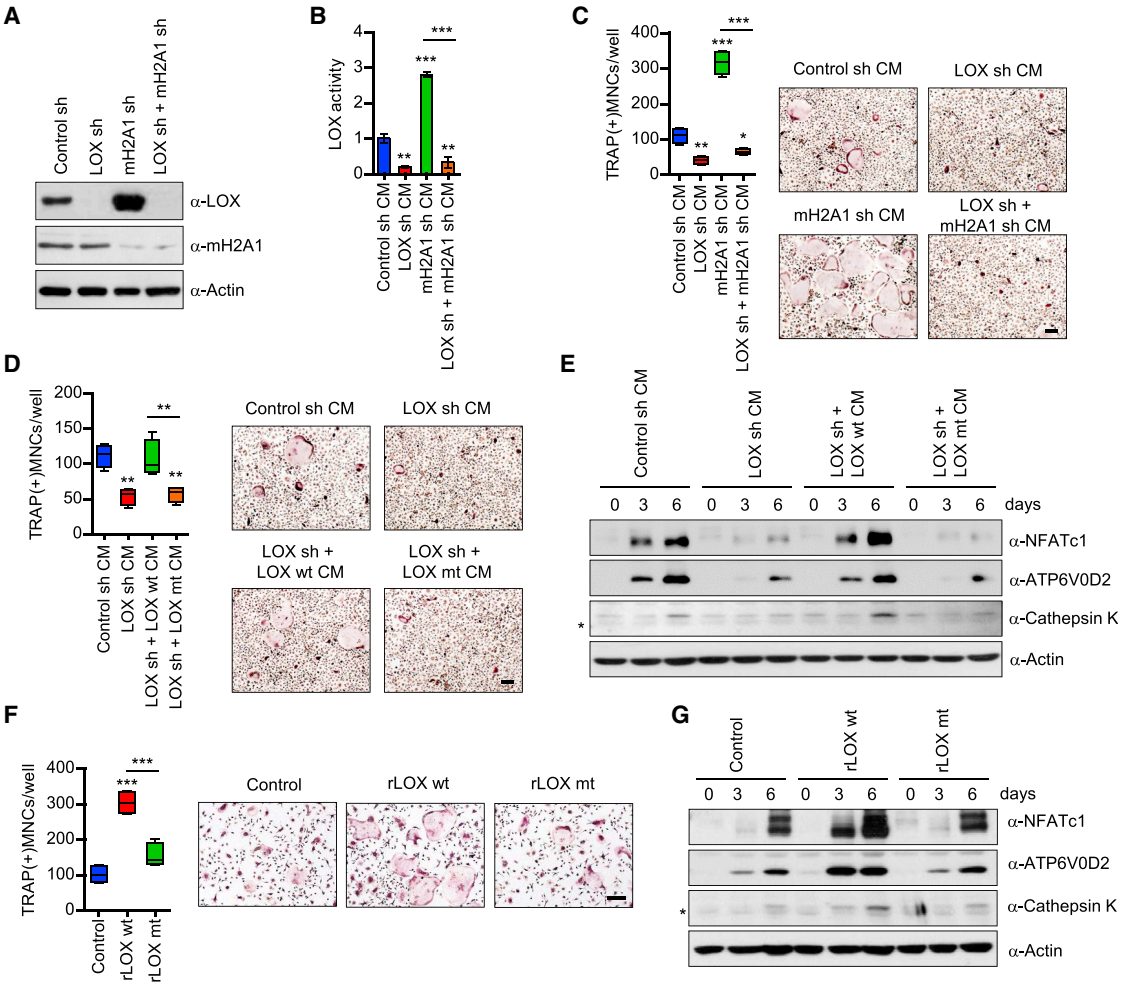

Figure 3. Dependence of mH2A1.2 Anti-osteoclastogenic Function on LOX

(A) Western blot analysis of lysates from MDA-MB-468 breast cancer cells expressing a control, LOX, or mH2A1 shRNA using the indicated antibodies.

(B) CMs were collected from MDA-MB-468 breast cancer cells depleted of LOX and/or mH2A1 and were used to measure LOX enzymatic activity as described in the Experimental Procedures.

(C) OCP cells were treated with CMs from MDA-MB-468 cells depleted of LOX and mH2A1 individually or together for 6 days. TRAP-positive multinucleated osteoclasts were stained (right) and counted (left). Scale bar, 100 μm.

(D) Osteoclast differentiation assays were carried out as in (C), but using CMs from LOX-depleted MDA-MB-468 cells expressing shRNA-resistant LOX wild-type (LOX wt) or oxidase-dead mutant (LOX mt). Scale bar, 100 μm.

(E) After treating OCP cells with MDA-MB-468 CMs as in (D), altered expression of NFATc1, ATP6V0D2, and cathepsin K was analyzed by western blot. β-Actin was used as a loading control. Non-specific band was marked by asterisk.

(F) OCP cells were treated with recombinant LOX (rLOX) wt or rLOX mt for 0, 3, and 6 days. Changes in osteoclast differentiation were assessed by TRAP staining (right) and counting (left). Scale bar, 100 μm.

(G) Western blot analyses of expression levels of NFATc1, ATP6V0D2, and cathepsin K after treating OCP cells with rLOX wt or rLOX mt. Error bars in (B)–(D) and (F) represent the means ± SD (n = 4) of three independent experiments; *p < 0.05, **p < 0.01, ***p < 0.001 (ANOVA analysis).

treatment on their capacity to resorb bone. Consistent with previous observations (Cox et al., 2015; Tsukasaki et al., 2017), rLOX-enhanced osteoclast formation increased the rate of bone resorption, stimulating the formation of resorption pits (Figure 4A). To further characterize the involvement of LOX in osteoclastogenesis and investigate the effect of rLOX treatment *in vivo*, we injected rLOX into the periosteal regions of female mouse calvaria once daily for 10 days. Our microscopic analysis of bone sections from rLOX-treated mice showed that treating mice with rLOX wt generated an apparent increase in the size of bone cavities (Figure 4B). Moreover, the fact that mice treated with rLOX mt display minimal changes in bone cavities strongly argues that LOX enzymatic function is required for enhancing bone destruction (Figure 4B). The observed changes in bone cavity were due to enhanced osteoclast differentiation, because higher numbers of TRAP-positive osteoclasts were detected in rLOX wt-injected mice compared to control and rLOX mt-treated mice in our histomorphometric analysis (Figure 4C). Consistent

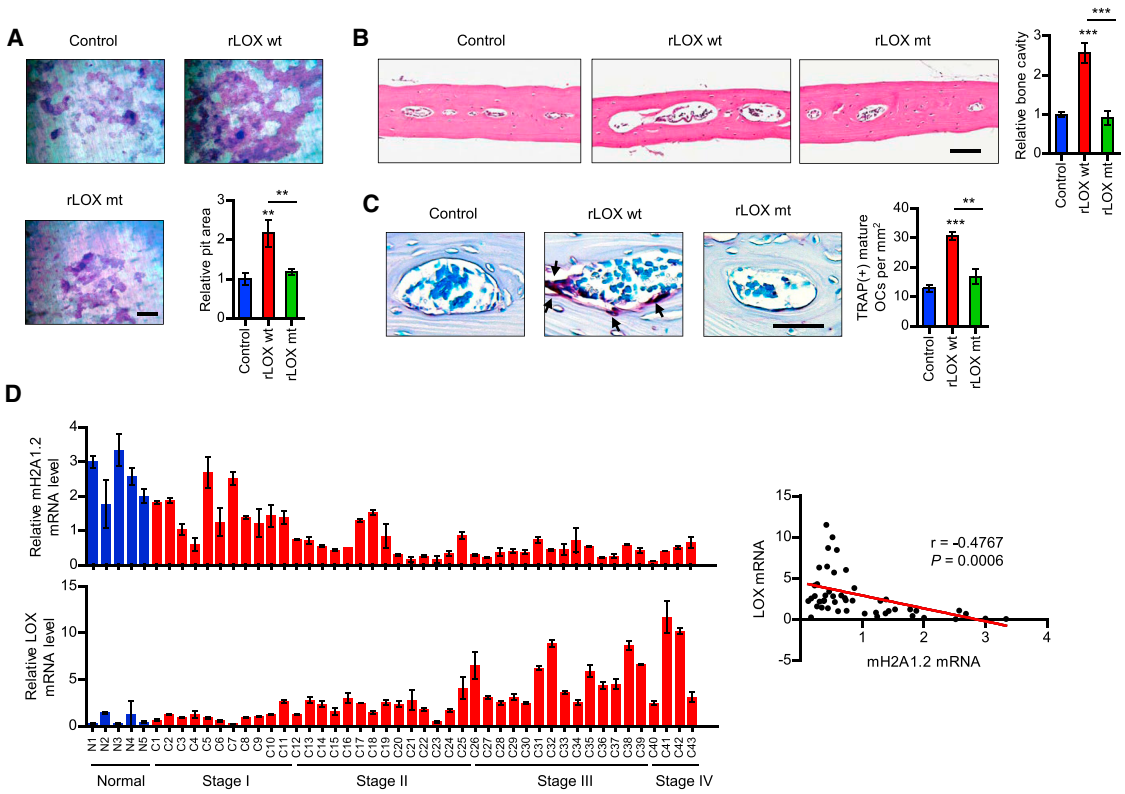

Figure 4. LOX-Mediated Stimulation of Osteoclastogenesis and Bone Resorption

(A) Osteoclasts were placed on dentin slices and cultured with MDA-MB-468 CMs in the presence of vehicle (control), rLOX wt, or rLOX mt for 48 hr. The dentin slices were stained for toluidine blue and analyzed for resorption pit area (lower right). Scale bar, 100 μm.

(B and C) Calvarial bones from C57BL/6 mice treated with vehicle (control), rLOX wt or rLOX mt were fixed, embedded, and subjected to sectioning, TRAP staining, and histological analysis. H&E staining analyses of bone lesions in C57BL/6 mice treated with vehicle (control), rLOX wt or rLOX mt are shown in (B). Representative images of TRAP-staining (scale bar, 100 μm) and quantification of TRAP-positive cells are shown in (C). Arrows point to TRAP-positive mature osteoclasts.

(D) Breast cancer TissueScan cDNA arrays (OriGene) were analyzed for mH2A1.2 (upper) and LOX (lower) expression by qRT-PCR. The scatterplot diagram on the right shows the Pearson correlation analysis of the relationship between mH2A1.2 and LOX expression. Error bars in (A)–(D) represent the means ± SD (A and D; n = 3, B and C; n = 5); $^{**}p < 0.01$, $^{***}p < 0.001$ versus Control (ANOVA analysis).

with these observations and to further confirm the repressive function of mH2A1.2 in LOX expression, the mice treated with mH2A1-depleted MDA-MB-468 CMs showed higher levels of mature osteoclast formation and bone cavity as compared to the control mice group treated with mock-depleted MDA-MB-468 CMs (Figure S4).

Having established the importance of LOX gene silencing in mH2A1.2 function, we then measured the expression levels of mH2A1.2 and LOX in a cDNA array of 39 breast tumor and 9 normal samples by qPCR. Our analysis revealed that expression levels of mH2A1.2 were lower in ~90% of tumor samples compared with normal samples (Figure 4D). By contrast, ~80% of the tumor samples exhibited higher levels of LOX expression than their normal counterparts. When the two expression data were compared, we found that mH2A1.2 and LOX expression levels are inversely correlated in the large majority of the examined samples. It is also noteworthy that mH2A1.2 and LOX show more significant expression changes in advanced stages of breast cancer (Figure 4D). Collectively, these data indicate that dysregulated expression of mH2A1.2 and LOX is a common feature in breast cancer and could be used to predict a risk for breast cancer-induced bone loss.

c-Src Signaling Pathway Is a Critical Target of LOX

LOX activity is associated with the phosphorylation status of c-Src, which is a key regulator of cytoskeletal reorganization, migration, and bone resorption in osteoclasts (Payne et al., 2005; Soriano et al., 1991; Tanaka et al., 1996). Given that rLOX treatment facilitates osteoclast differentiation, we wondered whether c-Src phosphorylation is also affected by rLOX treatment. In order to check this possibility, we analyzed the levels of phosphorylated c-Src in OCP cells after rLOX treatment by western blot. OCP cells treated with rLOX wt exhibited higher levels of c-Src phosphorylation over a 30-min time period, as compared with those observed in mock-treated cells (Figure 5A). In the same experiment, c-Src phosphorylation levels were unchanged following the treatment with rLOX mt. We

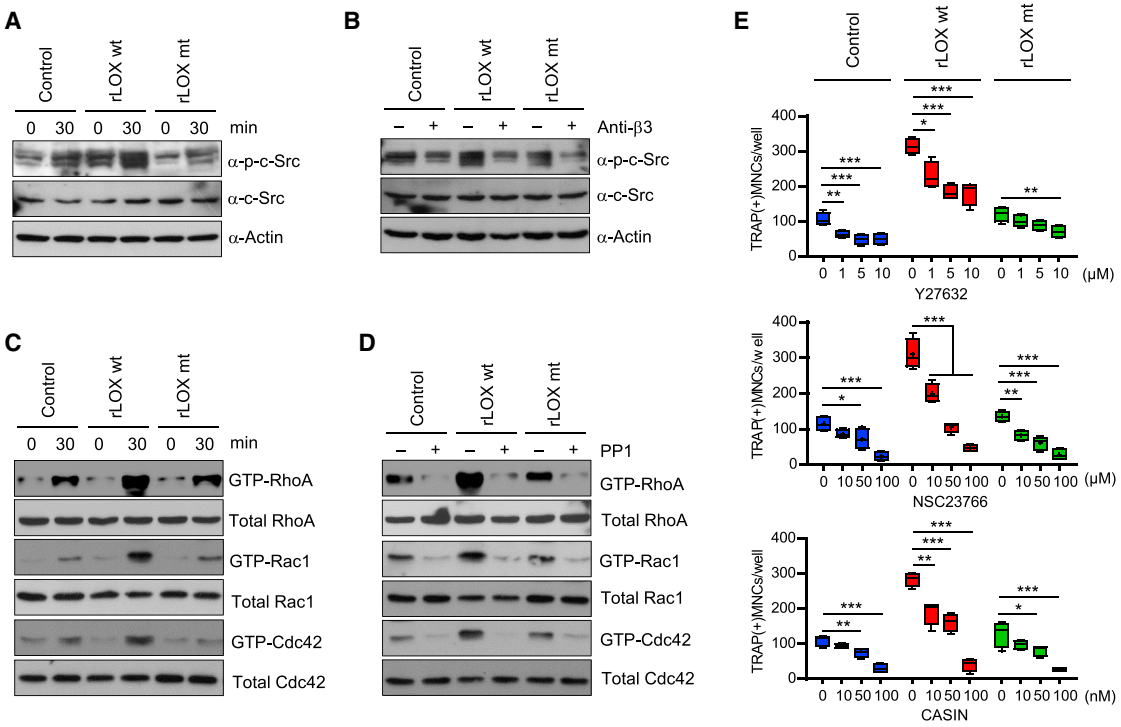

Figure 5. An Important Role for LOX in Facilitating c-Src Phosphorylation and Function

(A) OCP cells were seeded onto the culture dishes coated with rLOX wt or mt in MDA-MB-468 CMs for 30 min. Whole cell lysates were prepared and analyzed by western blot using antibodies recognizing c-Src and c-Src phosphorylation.

(B) After pretreating with function-blocking antibody against integrin β3 subunit, OCP cells were plated on the culture dishes coated with rLOX wt or rLOX mt in MDA-MB-468 CMs and incubated for 30 min. Whole cell lysates were prepared and analyzed by western blot as in (A).

(C) Small GTPase (RhoA/Rac1/Cdc42) assays were performed as in (A), and subjected to western blot analysis with antibodies against RhoA, Rac1, and Cdc42.

(D) Small GTPases assays were done as in (B, but using the Src inhibitor PP1.

(E) OCP cells were treated with rLOX wt or rLOX mt for 6 days in the presence of the indicated concentrations of RhoA inhibitor Y27632, Rac1 inhibitor NSC23766, or Cdc42 inhibitor CASIN. TRAP-positive multinucleated osteoclasts were stained and counted. Error bars represent the means ± SD (n = 4); *p < 0.05, **p < 0.01, ***p < 0.001 (ANOVA analysis).

next wanted to know how LOX-mediated extracellular matrix remodeling can stimulate phosphorylation of c-Src. As integrins are known to mediate interactions between the extracellular and intracellular environments (Guo and Giancotti, 2004), they are good candidates for transducing LOX-mediated signals. Activation of integrin αvβ3 is known to promote c-Src phosphorylation in osteoclasts via an ''outside-in'' signaling mechanism (Faccio et al., 2003; Geiger et al., 2001). Therefore, we investigated whether integrin αvβ3 was involved in transducing the effects of extracellular LOX activity to intracellular c-Src phosphorylation using a function-blocking antibody against integrin β3 subunit. Treatment with this blocking antibody reduced the levels of phosphorylated c-Src in OCP cells seeded onto the culture wells coated with rLOX wt or rLOX mt in MDA-MB-468 CMs (Figure 5B). These results suggest that LOX-mediated ECM remodeling may induce activation of integrin β3 and phosphorylation of c-Src kinase.

Considering that the Rho family small GTPases (RhoA, Rac1, and Cdc42) are downstream effectors of integrin αvβ3 activation and c-Src signaling (Faccio et al., 2003), we also investigated the levels of active GTP-bound forms of RhoA, Rac1, and Cdc42 in osteoclasts seeded onto on the culture plates coated with rLOX wt or rLOX mt in MDA-MB-468 CMs. The results of this effort indicated that levels of GTP-bound RhoA, Rac1, and Cdc42 are significantly increased after treatments with rLOX wt, but not rLOX mt (Figure 5C). Our western blot analysis also revealed lower levels of active GTP-bound RhoA, Rac1, and Cdc42 after treatments with c-Src inhibitor PP1 (Figure 5D), suggesting that small GTPase signaling pathways are downstream effectors of LOX-mediated c-Src activation. Consistent with these results, when the effects of small molecule inhibitors targeting RhoA (Y27632), Rac1 (NSC23766), and Cdc42 (CASIN) on rLOX-enhanced osteoclastogenesis were evaluated, OCP cell differentiation was reduced significantly after NSC23766 or CASIN treatment and moderately after Y27632 treatment (Figure 5E). These results support the view that LOX-stimulated osteoclastogenesis is dependent on signaling pathways involving RhoA, Rac1, and Cdc42. As mH2A1.2 has a role in inhibiting LOX gene expression and osteoclastogenic function, mH2A1-depleted MDA-MB-468 CMs might therefore be expected to exhibit upregulation in c-Src phosphorylation and function. Indeed, when we repeated the above experiments using control and mH2A1-depleted MDA-MB-468 CMs and compared their effects, we clearly observed stronger responses

to mH2A1-depleted MDA-MB-468 CMs as compared with control MDA-MB-468 CMs (Figure S5).

OCP cell migration is a prerequisite for cell-cell contact and fusion prior to the formation of multinuclear osteoclasts. Because small GTPases are important players in controlling this differentiation process (Kim et al., 2016a), a potential role for LOX in OCP cell migration was investigated by using RhoA, Rac1, and Cdc42 inhibitors. The results showed that treating OCP cells with rLOX wt stimulated migration, but antagonizing RhoA, Rac1, and Cdc42 GTPase activities with their inhibitors impeded OCP cell migration (Figure S3H). Because small GTPases play important roles in controlling invasion properties of cancer cells, which is linked to LOX function (Erler et al., 2006; Gómez del Pulgar et al., 2005), rLOX-treated MDA-MB-468 cells were subjected to cell invasion assays after exposure to RhoA, Rac1, and Cdc42 inhibitors. Transfection of rLOX wt promoted MDA-MB-468 cell invasion, but rLOX mt showed no invasion-promoting activity (Figure S3I). Importantly, exposure of rLOX-treated cells to RhoA, Rac1, and Cdc42 inhibitors attenuated their invasion capacity, albeit to different extents (Figure S3I). These repressive patterns were also observable after exposing control or rLOX mt-treated cells to the inhibitors, but to a much less severe degree. These data overall support the notion that the small GTPases signaling plays a critical role in LOX-mediated OCP cell migration and breast cancer cell invasion.

EZH2 Binds to mH2A1.2 Nucleosomes and Establishes LOX G Silencing in Breast Cancer Cells

Several recent studies, including ours, suggested that mH2A incorporation into nucleosomes influences histone modification patterns associated with transcriptional silencing or activation (Chen et al., 2014; Douet et al., 2017; Gamble et al., 2010; Gaspar-Maia et al., 2013; Kim et al., 2013). Thus, we asked whether any histone modifications are altered in mH2A1.2 nucleosomes and play a role, if any, mH2A1.2-induced gene silencing in MDA-MB-468 breast cancer cells. To this end, MDA-MB-468 cells were stably transfected with expression vectors encoding FLAG-tagged H2A or mH2A1.2 (Figure 6A). After confirming the comparable expression of ectopic H2A and mH2A1.2 in transfected cells (data not shown), soluble chromatin was prepared and digested with micrococcal nuclease to yield mainly mononucleosomes. Mononucleosomes containing ectopic histones were then purified by immunoprecipitations with anti-FLAG antibody under stringent conditions (300 mM KCl and 0.2% NP40). Coomassie blue staining confirmed stoichiometry of H2A, H2B, H3, and ectopic H2A/mH2A1.2 in the purified nucleosomes (Figure 6A). In checking the states of histone acetylation and methylation of purified nucleosomes by western blot, we detected much higher levels of H3K27me3 in mH2A1.2 nucleosomes than in H2A nucleosomes (Figure 6A). Consistent with its role in transcriptional repression, mH2A1.2 nucleosomes retained lower levels of three active histone marks, H3ac, H4ac, and H3K4me3. Contrarily, other histone modifications did not show any significant differences between H2A and mH2A1.2 nucleosomes. These results are consistent with the previous observation that H3K27me3 is a dominant histone modification in mH2A nucleosomes and mH2A-enriched genomic regions (Buschbeck et al., 2009; Gamble et al., 2010). Along with a recent demonstration of H3K27me3 being most highly increased in breast cancer cells (Leroy et al., 2013), this finding also suggests a possible role for H3K27me3 in mH2A1.2-induced gene silencing in MDA-MB-468 cells. To investigate this possibility, we suppressed the expression of EZH2 that is mainly responsible for H3K27me3 in breast cancer cells (Leroy et al., 2013) and evaluated its impact on LOX gene transcription. Relative to non-targeting control shRNA, shRNA directed against EZH2 efficiently depleted EZH2 and almost completely abrogated H3K27me3 in MDA-MB-468 cells (Figure 6B). This decrease in EZH2-mediated H3K27me3 generated a significant enhancement of LOX expression in the cells and thus LOX enzymatic activity in CMs (Figures 6B and 6C). The observed effects of EZH2 knockdown could be rescued by EZH2 wild-type, but not a methyltransferase-dead mutant (Figures 6B and 6C), strongly supporting that EZH2 enzymatic activity is critical for mH2A1.2 function in repressing LOX expression.

The fact that EZH2 catalyzes H3K27me3 in mH2A1.2-dependent manner led us to propose that EZH2 can recognize and bind mH2A1.2 nucleosomes in MDA-MB-468 cells. An initial western blot analysis showed, as predicted, that EZH2 is co-purified with mH2A1.2 nucleosomes from MDA-MB-468 breast cancer cells (Figure 6D). Because there was no detectable binding of EZH2 to H2A nucleosomes, the observed binding was specific and occurred through mH2A1.2. These data were supported by our finding that mH2A1 antibody is able to coimmunoprecipitate endogenous EZH2 from lysates of MDA-MB-468 breast cancer cells (Figure 6E). The observed interaction was further verified by reciprocal immunoprecipitation using EZH2 antibody (Figure 6E). To more precisely determine the nature of the observed interactions, we also carried out a series of glutathione S-transferase (GST) pull down assays. In clear confirmation of a direct interaction, EZH2 bound strongly to GST-mH2A1.2 but not to GST (Figure 6F). In similar binding experiments with truncated versions of mH2A1.2, the C-terminal macrodomain of mH2A1.2 (residues 123–371) still interacted with EZH2 (Figure 6F). However, N-terminal histone domain (residues 1–122) failed to show any affinity for EZH2, indicating that the binding of mH2A1.2 to EZH2 is dependent upon its C-terminal macrodomain. In mapping mH2A1.2-interacting region of EZH2, the binding of the N-terminal region (residues 1–250) of EZH2 was readily detectable, but its central and C-terminal regions (residues 251–500 and 501–746) showed no interactions with mH2A1.2 under the same assay conditions (Figure 6F). To identify amino acid residues critical for the mH2A1.2-EZH2 interaction, we next generated a structural model of the mH2A1.2-EZH2 complex based on their crystal structures (Justin et al., 2016; Kustatscher et al., 2005) using the program Cluspro 2.0 (Kozakov et al., 2017). Our model suggested that E254 of mH2A1.2 is positioned to contact N45 and K48 of EZH2. Moreover, L56 of EZH2 was predicted to be in hydrophobic contacts with V278 and N317 of mH2A1.2 (Figure 6G). Consistent with this model, *in vitro* binding assays employing mH2A1.2 E254A and EZH2 L56A mutant proteins demonstrated that the mH2A1.2-EZH2 interaction was significantly inhibited by either mutation (Figure 6H).

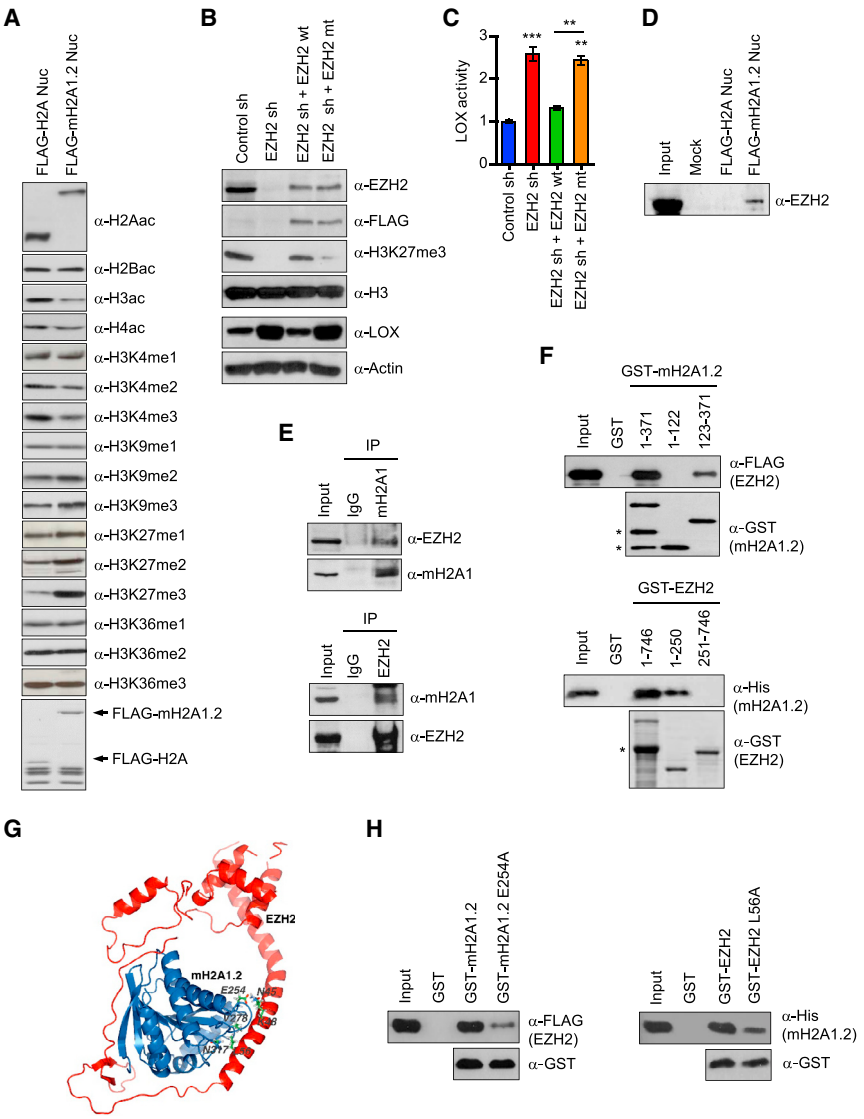

Figure 6. Selective Recognition and Modification of mH2A1.2 Nucleosomes by EZH2

(A) Mononucleosomes were prepared from MDA-MB-468 cells transfected with FLAG-H2A or FLAG-mH2A1.2 expression vector as described (Kim et al., 2013). FLAG-H2A and FLAG-mH2A1.2 nucleosomes were immunoprecipitated and analyzed by western blotting with antibodies specific for the indicated histone modifications. The bottom panel shows a Coomassie-stained gel of the purified nucleosomes.

(B) EZH2-depleted MDA-MB-468 cells were complemented with EZH2 wild-type (EZH2 wt) or methyltransferase-dead mutant (EZH2 mt), and relative levels of H3K27me3 and LOX expression were determined by western blot.

(C) LOX activity was measured in CMs collected from mock-depleted control or EZH2-depleted MDA-MB-468 cells. The rescue effects of EZH2 wt and mt on LOX activity were also analyzed. Error bars represent the means ± SD (n = 3); **p < 0.01, ***p < 0.001 versus Control sh (ANOVA analysis).

(D) Mononucleosomes containing ectopic H2A or mH2A1.2 were purified as in (A) and subjected to western blotting with EZH2 antibody.

(E) MDA-MB-468 cell extracts were immunoprecipitated with mH2A1 and EZH2 antibodies and analyzed by western blot. Ten percent of the input proteins were also examined by western blotting.

(F) FLAG-EZH2 and His-mH2A1.2 were incubated with the indicated GST-mH2A1.2 and GST-EZH2 fusions. After extensive washing, bound EZH2 and mH2A1.2 proteins were analyzed by western blot. Non-specific bands were marked by asterisks.

(G) The model of mH2A1.2-EZH2 interaction was built on the basis of PDB entries 1zr5 (mH2A1.2) and 5hyn (EZH2) in docking simulations using the program Cluspro 2.0. The chosen docking prediction is shown with the EZH2 (L56) and mH2A1.2 (V278, N317) side chains in ball-and-stick representation.

(H) GST pull-down assays were conducted as in (F), except that GST-mH2A1.2 and GST-EZH2 carrying the indicated point mutations were used.

EZH2 Localizes at the *LOX* Locus and Impairs Osteoclastogenesis in a mH2A1.2-Dependent Fashion

We next initiated efforts to examine the significance of EZH2-mH2A1.2 interaction in establishing and maintaining a repressive chromatin environment over the *LOX* locus. We hypothesized that this LOX gene-targeted activity in MDA-MB-468 breast cancer cells confers anti-osteoclastogenic properties to EZH2. In an attempt to test this hypothesis, we prepared CMs from MDA-MB-468 cells depleted of EZH2 and explored their effects on OCP cell differentiation into osteoclasts. Our analysis clearly showed that knockdown of EZH2 in MDA-MB-468 cells endowed CMs with the ability to stimulate osteoclast differentiation (Figure 7A). Ectopic expression of EZH2 wild-type, but not the enzymatically dead mutant, in EZH2-depleted MDA-MB-468 cells restored OCP cell differentiation to levels quantitatively similar to those observed with mock-depleted control cell CMs—indicative of the importance of EZH2 methyltransferase activity (Figure 7B). Importantly, knockdown of EZH2 in mH2A1-depleted cells failed to increase the osteoclastogenic activity of CMs, indicative of mH2A1-dependent function of EZH2 in breast cancer cells (Figure 7A). It was also apparent that depleting EZH2 accelerated OCP cell migration and MDA-MB-468 cell invasion dependently of mH2A1 (Figure S6). The inhibitory effects of EZH2 on osteoclastogenesis were also verified by monitoring changes in the expression of NFATc1, ATP6V0D2, and cathepsin K genes in response to knockdown and rescue of EZH2 in MDA-MB-468 cells (Figure 7C). Moreover, and as shown in Figures 7D and 7E, we confirmed by ChIP assay that *LOX* gene harbors high levels of EZH2 and H3K27me3 and loses H3K27me3 following EZH2 knockdown. The observed enrichment of EZH2 largely disappeared upon concomitant depletion of mH2A1 (Figure 7D), again confirming the functional link between EZH2 and mH2A1.2 in *LOX* gene silencing.

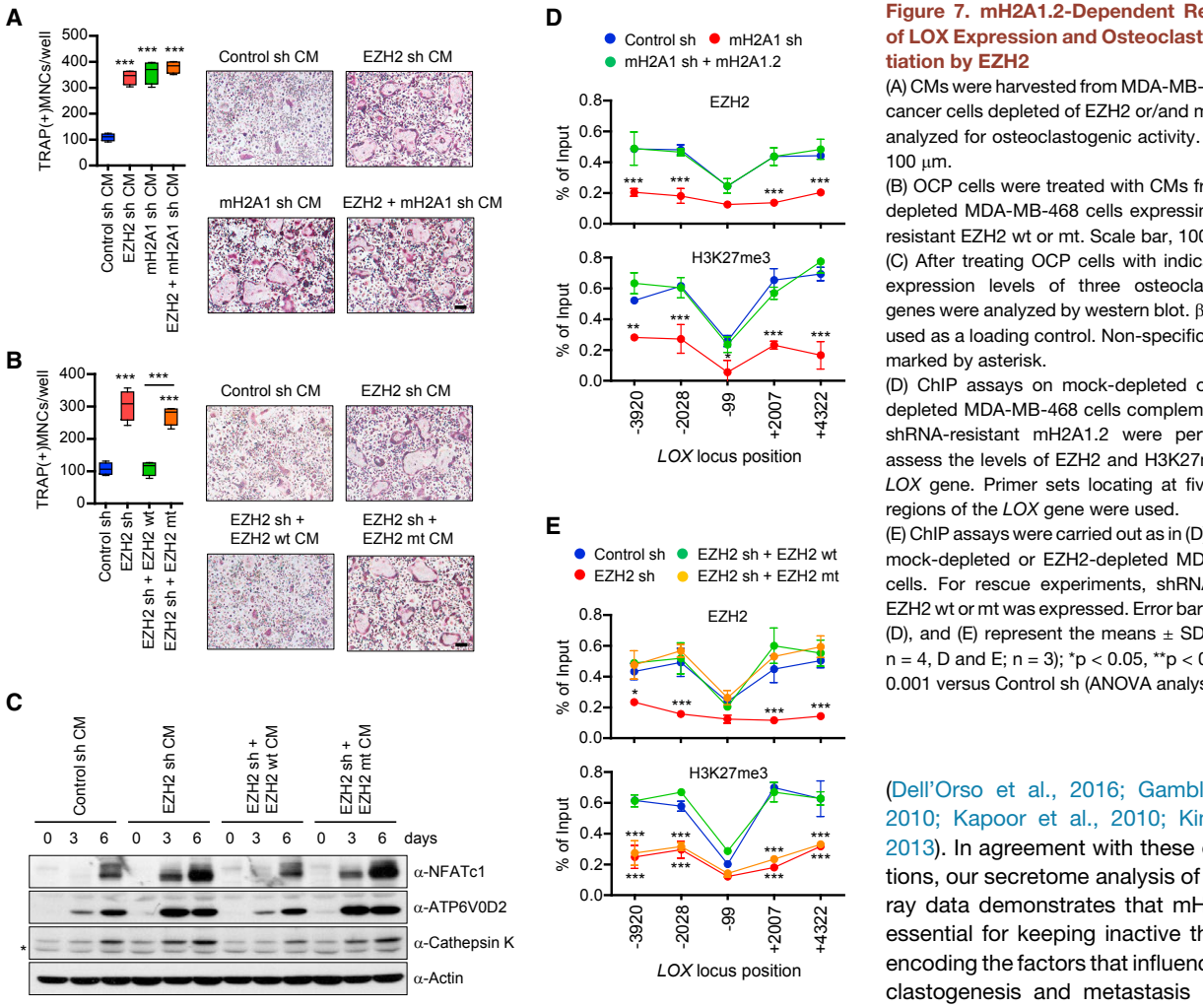

Figure 7. mH2A1.2-Dependent Repression of LOX Expression and Osteoclast Differentiation by EZH2

(A) CMs were harvested from MDA-MB-468 breast cancer cells depleted of EZH2 or/and mH2A1 and analyzed for osteoclastogenic activity. Scale bar, 100 μm.

(B) OCP cells were treated with CMs from EZH2-depleted MDA-MB-468 cells expressing shRNA-resistant EZH2 wt or mt. Scale bar, 100 μm.

(C) After treating OCP cells with indicated CMs, expression levels of three osteoclast marker genes were analyzed by western blot. β-Actin was used as a loading control. Non-specific band was marked by asterisk.

(D) ChIP assays on mock-depleted or mH2A1-depleted MDA-MB-468 cells complemented with shRNA-resistant mH2A1.2 were performed to assess the levels of EZH2 and H3K27me3 at the *LOX* gene. Primer sets locating at five different regions of the *LOX* gene were used.

(E) ChIP assays were carried out as in (D), but using mock-depleted or EZH2-depleted MDA-MB-468 cells. For rescue experiments, shRNA-resistant EZH2 wt or mt was expressed. Error bars in (A), (B), (D), and (E) represent the means ± SD (A and B; n = 4, D and E; n = 3); *p < 0.05, **p < 0.01, ***p < 0.001 versus Control sh (ANOVA analysis).

DISCUSSION

While a considerable amount of data have accumulated over the last several years regarding osteoclastogenic potentials of cancer cell-secreted factors, a detailed mechanistic description for how the expression of these bone destructive factors is regulated in cancer cells is lacking. We undertook a systematic investigation of the mechanisms that are used to regulate these processes in breast cancer cells. As a model system for our study, we selected the ER$^+$ MDA-MB-468 cell, which is a moderately metastatic breast cancer cell. We also took advantage of an *in vitro* CM-based assay that circumvents some of the complications linked to *in vivo* studies. One important initial result obtained using this assay system was that mH2A1.2 significantly decreases osteoclastogenic potential of soluble factors secreted by MDA-MB-468 breast cancer cells. The observation that two other mH2A isoforms, mH2A1.1 and mH2A2, do not participate in regulating osteoclastogenesis is important in light of several recent reports suggesting that mH2A isoforms are dedicated to regulatory roles in specific gene expression (Dell'Orso et al., 2016; Gamble et al., 2010; Kapoor et al., 2010; Kim et al., 2013). In agreement with these observations, our secretome analysis of microarray data demonstrates that mH2A1.2 is essential for keeping inactive the genes encoding the factors that influence osteoclastogenesis and metastasis in MDA-MB-468 breast cancer cells. This study represents the first genome-wide expression profiling and secretome analysis of mH2A target genes, and establishes mH2A1.2 as a key player in stable epigenetic silencing of genes encoding secreted factors. Our ChIP and qRT-PCR assays using mH2A1-depleted cells rescued with ectopic mH2A1.2 also suggest that accurate enrichment of mH2A1.2 in target genes is vital to the control of secretory factor gene expression in MDA-MB-468 cells.

Because our secretome analysis of microarray data ranked LOX gene highest, and because LOX has been implicated in bone metastasis, we investigated the mechanism underlying the observed mH2A1.2-dependent phenomena by studying a role for mH2A1.2 in regulating LOX gene. It was shown that LOX is overexpressed and secreted from MDA-MB-231 breast cancer cells with high metastatic potential, and this secreted LOX is a critical player in this cancer cell bone metastasis (Cox et al., 2015). In highly metastatic MDA-MB-231 cells, mH2A1.2 is minimally expressed—contrary to what was observed in moderately metastatic MDA-MB-468 cells—and thus CMs from these cells may well facilitate osteoclast differentiation. In MDA-MB-468 cells, however, mH2A1.2 is highly expressed and constitute a repressive barrier to LOX expression, and it

needs to be removed from the LOX gene locus in order to activate LOX transcription. The exchange of canonical histones with histone variants is highly dynamic and can be modulated through a number of different mechanisms. Although the precise mechanism is unknown, the exchange of specific histone variants is shown to be promoted by specific patterns of posttranslational modifications. Thus, we are tempted to speculate that the ability of exchange factors to selectively incorporate mH2A1.2 into the LOX locus might be dependent on specific modification status of mH2A1.2. The osteoclastogenic function of LOX seems to be dependent on LOX-mediated collagen cross-linking, because the expression of LOX wild-type, but not LOX oxidase-dead mutant, in LOX-depleted cells restored CM-induced osteoclast differentiation rates. Notably, and consistent with recent studies (Cox et al., 2015; Tsukasaki et al., 2017), our investigation demonstrated that rLOX can recapitulate the osteoclastogenic properties *in vitro* and stimulate bone resorption *in vivo*. These findings underscore the importance of mH2A1.2 in the regulation of LOX expression and also suggest that accurate targeting of mH2A1.2 within the *LOX* gene locus may be vital for the control of breast cancer-induced osteoclastogenesis and its related physiological responses. In this regard, LOX is a promising target for novel therapeutic strategies, as rLOX treatments significantly stimulated bone resorption and osteoporosis. Our data also demonstrate that LOX likely facilitates breast cancer-induced osteoclast differentiation through the activation of extracellular matrix remodeling processes by upregulating Src phosphorylation and integrin signaling. Further, by inhibitor and blocking antibody treatments, we were able to confirm that Src phosphorylation and integrin signaling processes are mutually dependent in LOX-dependent osteoclastogenic reactions.

Another intriguing finding of our study is that mH2A1.2 nucleosomes are enriched with H3K27me3 in MDA-MB-468 breast cancer cells, underscoring the connection between mH2A1.2 and H3K27me3 in regulating breast cancer-induced generation of mature osteoclasts. Such a connection between mH2A1 and H3K27me3 has been also observed in previous studies (Buschbeck et al., 2009; Chen et al., 2014; Gamble et al., 2010); however, the mechanistic details for this observation have not been explored. Functionally, we demonstrate that EZH2 is responsible for generating H3K27me3 and acts as a negative regulator of LOX gene in MDA-MB-468 cells. EZH2 directly interacts and colocalizes with mH2A1.2 in the *LOX* gene locus and does so in a mH2A1.2 macrodomain-dependent fashion. Depletion of EZH2 substantially increased the osteoclastogenic capacity of CMs from MDA-MB-468 cells. mH2A1.2 fails to control LOX-triggered activation of osteoclast differentiation after EZH2 knockdown in MDA-MB-468 cells, indicating that the suppressive behavior of mH2A1.2 on CM-induced osteoclast differentiation is EZH2-dependent. Thus, mH2A1.2 constitutes a recruitment platform for EZH2 to mediate H3K27me3 and generate LOX inactivation, and it needs to be dissociated from *LOX* locus in order to remove H3K27me3 and activate *LOX* transcription during osteoclastogenic event. Mechanistically, such cooperative actions of mH2A1.2 and EZH2 should provide additional levels of efficiency and specificity to transcriptional manipulation of LOX gene in MDA-MB-468 cells. Because the expression of mH2A1.2 is mis-regulated in cell lines for other cancer types (Kim et al., 2013), it would be interesting to investigate whether a similar EZH2-dependent mechanism of mH2A1.2 action may also apply to other bone metastatic cancers.

Based on our observations, together with findings from previous studies, we present the following working model for how mH2A1.2 negatively regulates breast cancer-induced osteoclastogenesis (Figure S7). In an initial state, mH2A1.2 is highly expressed and localizes at LOX gene. Once incorporated into LOX gene, mH2A1.2 utilizes its macrodomain to recruit EZH2 through direct protein-protein interactions. An epigenetic gene silencing process involving H3K27me3 then takes place to keep LOX gene in an inactive state. In breast cancer cells, EZH2 functionally cooperates with mH2A1.2, such that facilitating its binding to mH2A could be a novel strategy for controlling LOX expression and thus breast cancer-induced osteoclastogenesis. Moreover, stimulating mH2A1.2 exchange reactions can enhance mH2A1.2-based localization of EZH2 over LOX gene locus and thus disrupt the active state of LOX expression and pathological oseteoclastogenesis.

EXPERIMENTAL PROCEDURES

Cell Culture and Osteoclast Differentiation

MDA-MB-468, MCF-7, MCF-10-2A, and MDA-MB-231 cells were purchased from the American Type Culture Collection. MDA-MB-468, MCF-7, and MDA-MB-231 cells were cultured in DMEM supplemented with 10% fetal bovine serum (FBS). MCF-10-2A cells were maintained in DMEM/F12 media with 20 ng/mL epidermal growth factor, 100 ng/mL cholera toxin, 0.01 mg/mL insulin, 500 ng/mL hydrocortisone, and 5% FBS. CMs were prepared by culturing cells to ~80% confluence, changing media to α-minimum essential medium (α-MEM) containing 0.5% FBS, and collecting media after 24 hr incubation. For osteoclast differentiation assays, bone marrow cells were isolated from 6-week-old C57BL/6 mice (The Jackson Laboratory) as recently described (Kim et al., 2016b) and in accordance with the University of Southern California guidelines. After priming the harvested cells with α-MEM containing 10% FBS and macrophage colony stimulating factor (M-CSF, 5 ng/mL) for 16 hr, non-adherent mononuclear cells were collected and cultured for an additional 3 days with α-MEM containing M-CSF (30 ng/mL) to generate primary osteoclast precursor (OCP) cells. OCP cells were then seed into a 48-well plate (2×10^4 cells/well) and grown in a 1:1 mixture of α-MEM culture medium and CMs supplemented with M-CSF (30 ng/mL) and RANKL (30 ng/mL) for 0, 3, or 6 days. The cells were fixed and stained with tartrate-resistant acid phosphatase (TRAP) using a leukocyte acid phosphatase staining kit (Sigma-Aldrich) according to manufacturer's instructions. TRAP-positive multinuclear cells with more than 3 nuclei were counted as osteoclasts under a light microscope.

Treatment and Analysis of Mice

Animal studies were conducted according to the guidelines set by the Institutional Animal Care and Use Committee. Female 6- to 8-week-old C57BL/6 mice were injected with 0.2 mg/kg rLOX or PBS alone onto their calvarias subcutaneously every other day. Five mice were injected for each group. 10 days after peptide injection, mice were euthanized, and calvaria were collected and immediately fixed with 3.7% formaldehyde. Paraffin-embedded samples were sectioned (6 μm thickness) and subjected to H&E and TRAP staining. Images were acquired with an Aperio ScanScope Model T3 and were analyzed with ImageScope software (Aperio Technologies). OCP cells (2×10^4 cells/well) were also treated with rLOX (100 ng/mL) along with RANKL (15 ng/mL) and M-CSF (30 ng/mL) and used to evaluate *in vitro* response to rLOX proteins.

For additional experimental materials and methods, see Supplemental Experimental Procedures.

DATA AND SOFTWARE AVAILABILITY

The accession number for the gene expression array data reported in this study is GEO: GSE107570.

SUPPLEMENTAL INFORMATION

Supplemental Information includes Supplemental Experimental Procedures, seven figures, and five tables and can be found with this article online at https://doi.org/10.1016/j.celrep.2018.06.020.

ACKNOWLEDGMENTS

This work was supported by the NIH (grant CA201561 awarded to W.A.). The study was also funded in part by pilot project grants from the Keck School of Medicine of USC.

AUTHOR CONTRIBUTIONS

J. Kim designed the experiments. W.A. provided guidance throughout. J. Kim, Y.S., S.L., M.K., V.P., J.F.L., H.S., K.K., T.S.U., J. Koh, D.J., and W.A. performed experiments and analyzed data. J. Kim and W.A. wrote the manuscript.

DECLARATION OF INTERESTS

The authors declare no competing interests.

Received: December 16, 2017
Revised: April 18, 2018
Accepted: June 3, 2018
Published: July 3, 2018

REFERENCES

Bild, A.H., Potti, A., and Nevins, J.R. (2006). Linking oncogenic pathways with therapeutic opportunities. Nat. Rev. Cancer *6*, 735–741.

Boyle, W.J., Simonet, W.S., and Lacey, D.L. (2003). Osteoclast differentiation and activation. Nature *423*, 337–342.

Buschbeck, M., Uribesalgo, I., Wibowo, I., Rué, P., Martin, D., Gutierrez, A., Morey, L., Guigó, R., López-Schier, H., and Di Croce, L. (2009). The histone variant macroH2A is an epigenetic regulator of key developmental genes. Nat. Struct. Mol. Biol. *16*, 1074–1079.

Chakravarthy, S., Gundimella, S.K., Caron, C., Perche, P.Y., Pehrson, J.R., Khochbin, S., and Luger, K. (2005). Structural characterization of the histone variant macroH2A. Mol. Cell. Biol. *25*, 7616–7624.

Chen, H., Ruiz, P.D., Novikov, L., Casill, A.D., Park, J.W., and Gamble, M.J. (2014). MacroH2A1.1 and PARP-1 cooperate to regulate transcription by promoting CBP-mediated H2B acetylation. Nat. Struct. Mol. Biol. *21*, 981–989.

Clézardin, P. (2011). Therapeutic targets for bone metastases in breast cancer. Breast Cancer Res. *13*, 207.

Cox, T.R., Rumney, R.M.H., Schoof, E.M., Perryman, L., Høye, A.M., Agrawal, A., Bird, D., Latif, N.A., Forrest, H., Evans, H.R., et al. (2015). The hypoxic cancer secretome induces pre-metastatic bone lesions through lysyl oxidase. Nature *522*, 106–110.

Dell'Orso, S., Wang, A.H., Shih, H.Y., Saso, K., Berghella, L., Gutierrez-Cruz, G., Ladurner, A.G., O'Shea, J.J., Sartorelli, V., and Zare, H. (2016). The histone variant macroH2A1.2 is necessary for the activation of muscle enhancers and recruitment of the transcription factor Pbx1. Cell Rep. *14*, 1156–1168.

Douet, J., Corujo, D., Malinverni, R., Renauld, J., Sansoni, V., Posavec Marjanović, M., Cantariño, N., Valero, V., Mongelard, F., Bouvet, P., et al. (2017). MacroH2A histone variants maintain nuclear organization and heterochromatin architecture. J. Cell Sci. *130*, 1570–1582.

Erler, J.T., Bennewith, K.L., Nicolau, M., Dornhöfer, N., Kong, C., Le, Q.T., Chi, J.T., Jeffrey, S.S., and Giaccia, A.J. (2006). Lysyl oxidase is essential for hypoxia-induced metastasis. Nature *440*, 1222–1226.

Erler, J.T., Bennewith, K.L., Cox, T.R., Lang, G., Bird, D., Koong, A., Le, Q.T., and Giaccia, A.J. (2009). Hypoxia-induced lysyl oxidase is a critical mediator of bone marrow cell recruitment to form the premetastatic niche. Cancer Cell *15*, 35–44.

Faccio, R., Novack, D.V., Zallone, A., Ross, F.P., and Teitelbaum, S.L. (2003). Dynamic changes in the osteoclast cytoskeleton in response to growth factors and cell attachment are controlled by beta3 integrin. J. Cell Biol. *162*, 499–509.

Gamble, M.J., Frizzell, K.M., Yang, C., Krishnakumar, R., and Kraus, W.L. (2010). The histone variant macroH2A1 marks repressed autosomal chromatin, but protects a subset of its target genes from silencing. Genes Dev. *24*, 21–32.

Gaspar-Maia, A., Qadeer, Z.A., Hasson, D., Ratnakumar, K., Leu, N.A., Leroy, G., Liu, S., Costanzi, C., Valle-Garcia, D., Schaniel, C., et al. (2013). MacroH2A histone variants act as a barrier upon reprogramming towards pluripotency. Nat. Commun. *4*, 1565.

Geiger, B., Bershadsky, A., Pankov, R., and Yamada, K.M. (2001). Transmembrane crosstalk between the extracellular matrix–cytoskeleton crosstalk. Nat. Rev. Mol. Cell Biol. *2*, 793–805.

Gómez del Pulgar, T., Benitah, S.A., Valerón, P.F., Espina, C., and Lacal, J.C. (2005). Rho GTPase expression in tumourigenesis: evidence for a significant link. BioEssays *27*, 602–613.

Guo, W., and Giancotti, F.G. (2004). Integrin signalling during tumour progression. Nat. Rev. Mol. Cell Biol. *5*, 816–826.

Henikoff, S., and Smith, M.M. (2015). Histone variants and epigenetics. Cold Spring Harb. Perspect. Biol. *7*, a019364.

Justin, N., Zhang, Y., Tarricone, C., Martin, S.R., Chen, S., Underwood, E., De Marco, V., Haire, L.F., Walker, P.A., Reinberg, D., et al. (2016). Structural basis of oncogenic histone H3K27M inhibition of human polycomb repressive complex 2. Nat. Commun. *7*, 11316.

Kang, Y., Siegel, P.M., Shu, W., Drobnjak, M., Kakonen, S.M., Cordón-Cardo, C., Guise, T.A., and Massagué, J. (2003). A multigenic program mediating breast cancer metastasis to bone. Cancer Cell *3*, 537–549.

Kapoor, A., Goldberg, M.S., Cumberland, L.K., Ratnakumar, K., Segura, M.F., Emanuel, P.O., Menendez, S., Vardabasso, C., Leroy, G., Vidal, C.I., et al. (2010). The histone variant macroH2A suppresses melanoma progression through regulation of CDK8. Nature *468*, 1105–1109.

Karsenty, G., Kronenberg, H.M., and Settembre, C. (2009). Genetic control of bone formation. Annu. Rev. Cell Dev. Biol. *25*, 629–648.

Kim, J.M., Heo, K., Choi, J., Kim, K., and An, W. (2013). The histone variant MacroH2A regulates Ca(2+) influx through TRPC3 and TRPC6 channels. Oncogenesis *2*, e77.

Kim, J.M., Kim, M.Y., Lee, K., and Jeong, D. (2016a). Distinctive and selective route of PI3K/PKCα-PKCδ/RhoA-Rac1 signaling in osteoclastic cell migration. Mol. Cell. Endocrinol. *437*, 261–267.

Kim, K., Punj, V., Kim, J.M., Lee, S., Ulmer, T.S., Lu, W., Rice, J.C., and An, W. (2016b). MMP-9 facilitates selective proteolysis of the histone H3 tail at genes necessary for proficient osteoclastogenesis. Genes Dev. *30*, 208–219.

Kozakov, D., Hall, D.R., Xia, B., Porter, K.A., Padhorny, D., Yueh, C., Beglov, D., and Vajda, S. (2017). The ClusPro web server for protein-protein docking. Nat. Protoc. *12*, 255–278.

Kustatscher, G., Hothorn, M., Pugieux, C., Scheffzek, K., and Ladurner, A.G. (2005). Splicing regulates NAD metabolite binding to histone macroH2A. Nat. Struct. Mol. Biol. *12*, 624–625.

Leroy, G., Dimaggio, P.A., Chan, E.Y., Zee, B.M., Blanco, M.A., Bryant, B., Flaniken, I.Z., Liu, S., Kang, Y., Trojer, P., and Garcia, B.A. (2013). A quantitative atlas of histone modification signatures from human cancer cells. Epigenetics Chromatin *6*, 20.

Maze, I., Noh, K.M., Soshnev, A.A., and Allis, C.D. (2014). Every amino acid matters: essential contributions of histone variants to mammalian development and disease. Nat. Rev. Genet. *15*, 259–271.

Payne, S.L., Fogelgren, B., Hess, A.R., Seftor, E.A., Wiley, E.L., Fong, S.F., Csiszar, K., Hendrix, M.J., and Kirschmann, D.A. (2005). Lysyl oxidase

regulates breast cancer cell migration and adhesion through a hydrogen peroxide-mediated mechanism. Cancer Res. *65*, 11429–11436.

Pehrson, J.R., and Fried, V.A. (1992). MacroH2A, a core histone containing a large nonhistone region. Science *257*, 1398–1400.

Raggatt, L.J., and Partridge, N.C. (2010). Cellular and molecular mechanisms of bone remodeling. J. Biol. Chem. *285*, 25103–25108.

Reynaud, C., Ferreras, L., Di Mauro, P., Kan, C., Croset, M., Bonnelye, E., Pez, F., Thomas, C., Aimond, G., Karnoub, A.E., et al. (2017). Lysyl oxidase is a strong determinant of tumor cell colonization in bone. Cancer Res. *77*, 268–278.

Soriano, P., Montgomery, C., Geske, R., and Bradley, A. (1991). Targeted disruption of the c-src proto-oncogene leads to osteopetrosis in mice. Cell *64*, 693–702.

Tanaka, S., Amling, M., Neff, L., Peyman, A., Uhlmann, E., Levy, J.B., and Baron, R. (1996). c-Cbl is downstream of c-Src in a signalling pathway necessary for bone resorption. Nature *383*, 528–531.

Teitelbaum, S.L., and Ross, F.P. (2003). Genetic regulation of osteoclast development and function. Nat. Rev. Genet. *4*, 638–649.

Tsukasaki, M., Hamada, K., Okamoto, K., Nagashima, K., Terashima, A., Komatsu, N., Win, S.J., Okamura, T., Nitta, T., Yasuda, H., et al. (2017). LOX fails to substitute for RANKL in osteoclastogenesis. J. Bone Miner. Res. *32*, 434–439.

Turner, J.M., Burgoyne, P.S., and Singh, P.B. (2001). M31 and macroH2A1.2 colocalise at the pseudoautosomal region during mouse meiosis. J. Cell Sci. *114*, 3367–3375.

Weilbaecher, K.N., Guise, T.A., and McCauley, L.K. (2011). Cancer to bone: a fatal attraction. Nat. Rev. Cancer *11*, 411–425.

Yin, J.J., Pollock, C.B., and Kelly, K. (2005). Mechanisms of cancer metastasis to the bone. Cell Res. *15*, 57–62.

Zaidi, M. (2007). Skeletal remodeling in health and disease. Nat. Med. *13*, 791–801.

Zhang, Y.X., Sun, H.L., Liang, H., Li, K., Fan, Q.M., and Zhao, Q.H. (2015). Dynamic and distinct histone modifications of osteogenic genes during osteogenic differentiation. J. Biochem. *158*, 445–457.

Cell Reports, Volume *24*

Supplemental Information

Regulation of Breast Cancer-Induced Osteoclastogenesis by MacroH2A1.2 Involving EZH2-Mediated H3K27me3

Jinman Kim, Yonghwan Shin, Sunyoung Lee, Miyeong Kim, Vasu Punj, Jason F. Lu, Hongin Shin, Kyunghwan Kim, Tobias S. Ulmer, Jungmin Koh, Daewon Jeong, and Woojin An

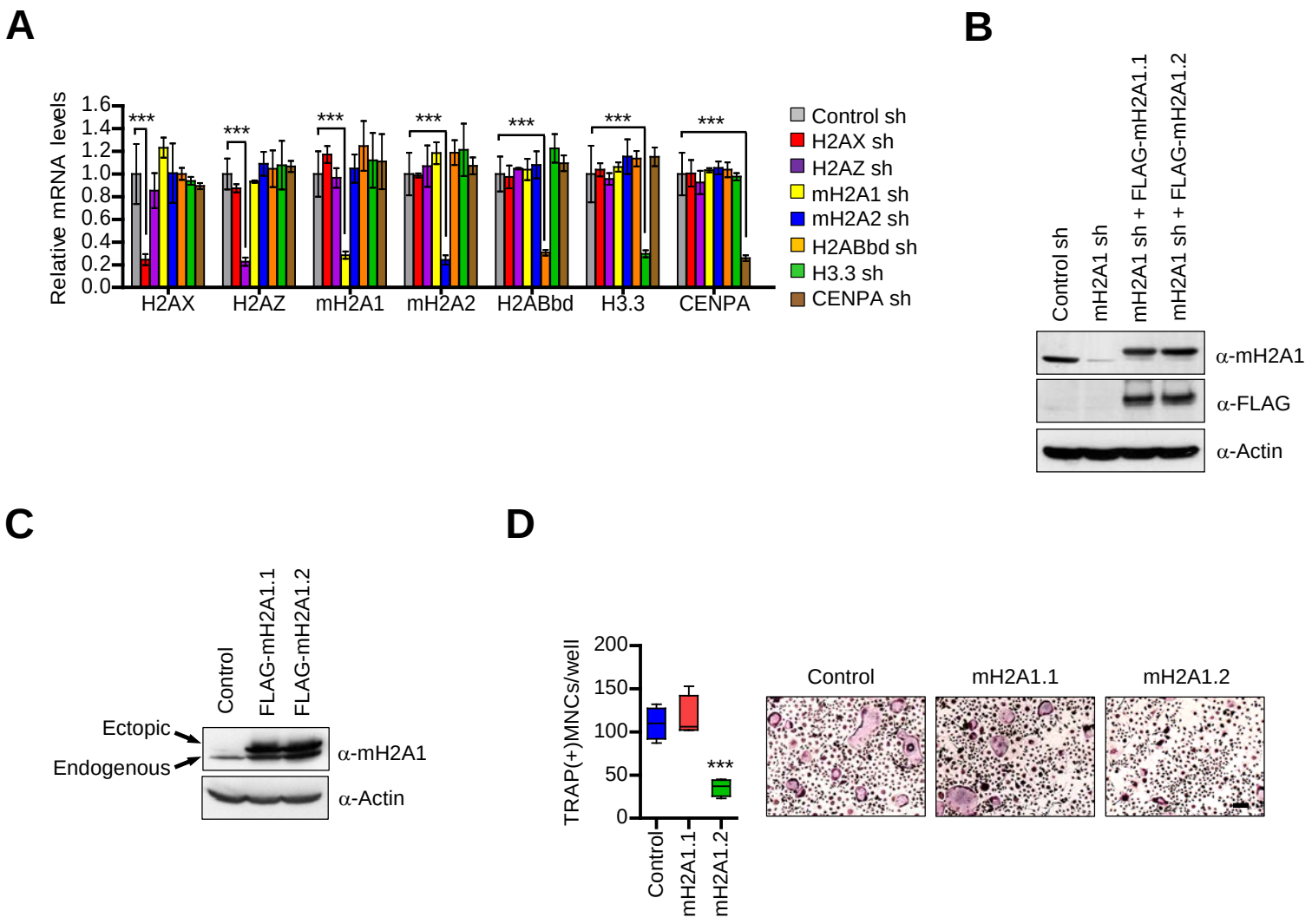

Figure S1. Validation of Knockdown/Re-expression and Osteoclastogenic Effects of mH2A1.2-Transfected cell CMs. Related to Figure 1. (A) MDA-MB-468 breast cancer cells were transduced with the indicated lentiviral shRNAs, and knockdown efficiency and specificity were determined by qRT-PCR with primers listed in Supplemental information. Error bars represent the means ± SD (n = 3); ***P<0.001 versus Control sh (ANOVA analysis). (B) Whole cell extracts were prepared from mH2A1-depleted MDA-MB-468 cells transfected with FLAG-mH2A1.1 or FLAG-mH2A1.1, and analyzed by Western blot using mH2A1, FLAG and β-Actin antibodies. (C) Western blot analysis showing comparable expression of ectopic mH2A1.1 and mH2A1.2 in MDA-MB-468 cells. (D) OCP cells were treated with CMs from control or mH2A1/mH2A2-transfected MDA-MB-468 cells for 6 days and stained for TRAP to analyze osteoclast differentiation. Scale bar, 100 μm. Error bars represent the means ± SD (n = 4); ***P<0.001 versus Control (ANOVA analysis).

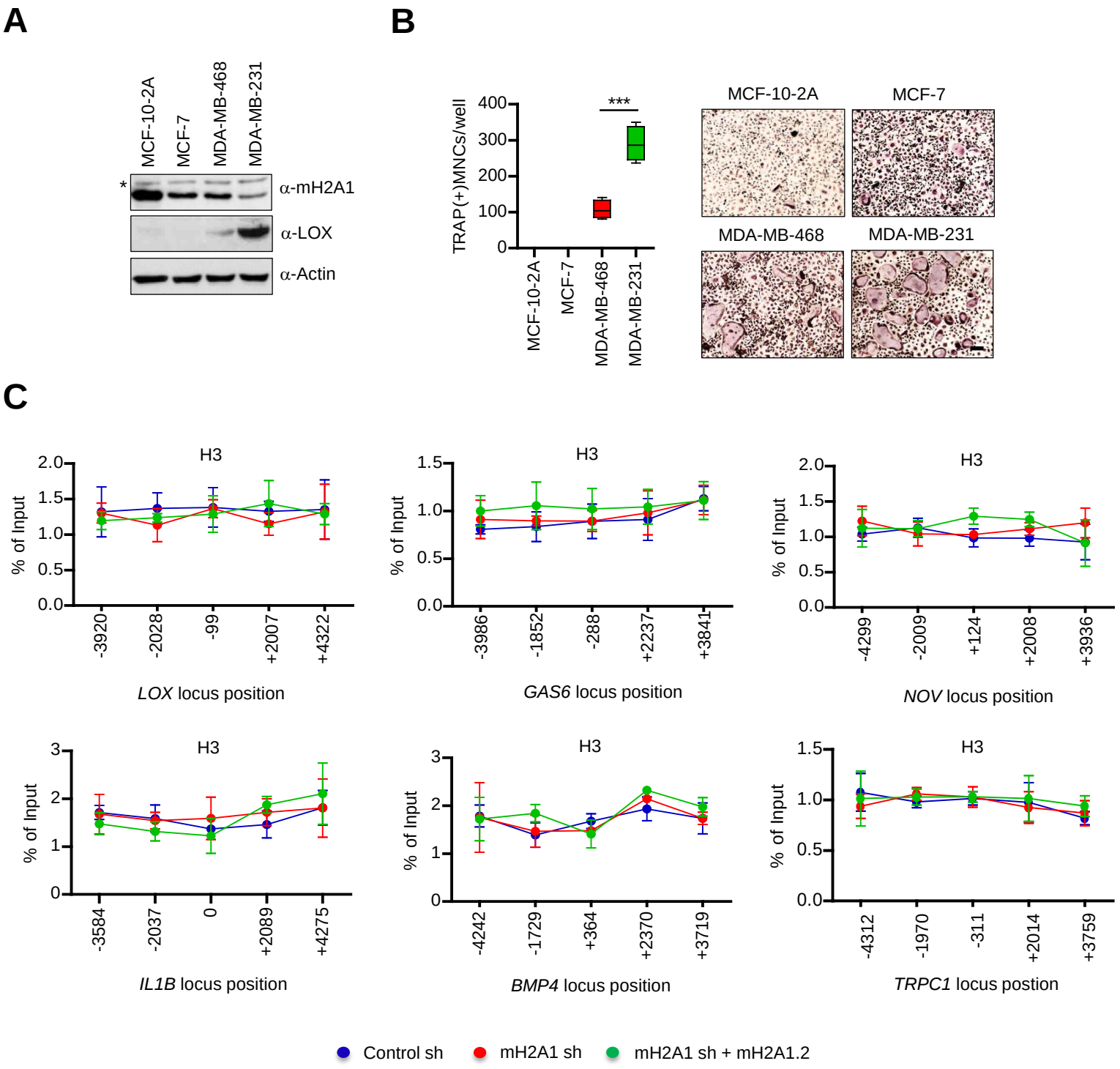

Figure S2. mH2A1 and Lox Expression Levels in Breast Cell Lines and H3 Levels at mH2A1.2 Target Genes. Related to Figure 2. (A) Whole cell lysates were prepared from MCF-10-2A, MCF-7, MDA-MB-468 and MDA-MB-231 cells, and analyzed by Western blot using mH2A1 and LOX antibodies. The asterisk indicates non-specific bands. (B) Osteoclastogenic properties of CMs from MCF-10-2A, MCF-7, MDA-MB-468 and MDA-MB-231 cells were measured by TRAP staining. Scale bar, 100 μm. Error bars represent the means ± SD (n = 4); ***P<0.001 (ANOVA analysis). (C) ChIP assays on mock-depleted or mH2A1-depleted MDA-MB-468 cells complemented with shRNA-resistant mH2A1.2 were performed to assess the levels of H3 at the *LOX*, *GAS6*, *NOV*, *IL1B*, *BMP4*, *TRPC1* genes. Error bars represent the means ± SD (n = 3).

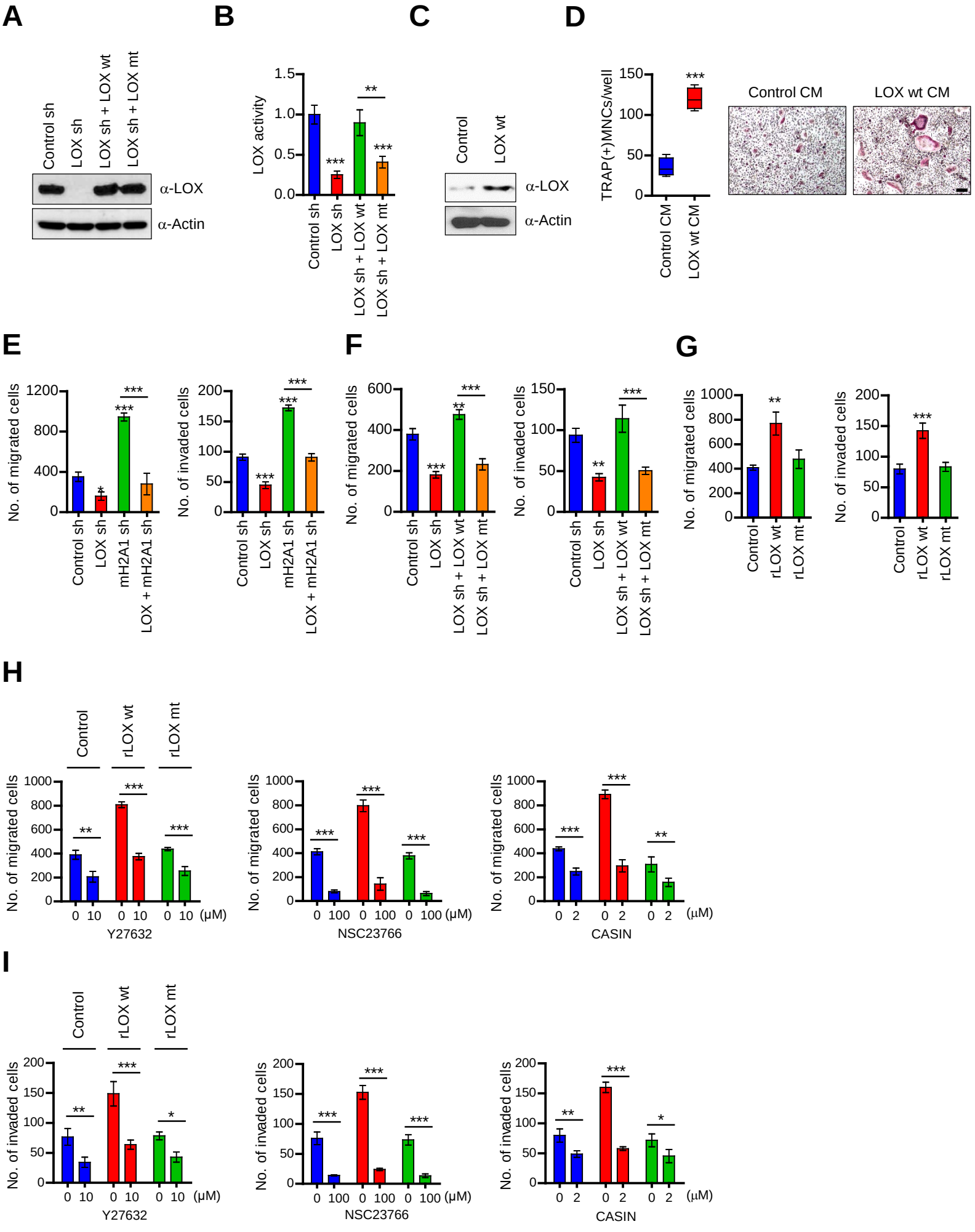
A
Control sh
LOX sh
LOX sh + LOX wt
LOX sh + LOX mt
α-LOX
α-Actin
B
LOX activity
1.5
1.0
0.5
0.0
**
***
***
Control sh
LOX sh
LOX sh + LOX wt
LOX sh + LOX mt
C
Control
LOX wt
α-LOX
α-Actin
D
TRAP(+)MNCs/well
150
100
50
0
***
Control CM
LOX wt CM
Control CM
LOX wt CM
E
No. of migrated cells
1200
800
400
0
***
***
*
Control sh
LOX sh
mH2A1 sh
LOX + mH2A1 sh
No. of invaded cells
200
150
100
50
0
***
***
***
Control sh
LOX sh
mH2A1 sh
LOX + mH2A1 sh
F
No. of migrated cells
600
400
200
0
***
***
**
Control sh
LOX sh
LOX sh + LOX wt
LOX sh + LOX mt
No. of invaded cells
150
100
50
0
**
***
Control sh
LOX sh
LOX sh + LOX wt
LOX sh + LOX mt
G
No. of migrated cells
1000
800
600
400
200
0
**
Control
rLOX wt
rLOX mt
No. of invaded cells
200
150
100
50
0
***
Control
rLOX wt
rLOX mt
H
Control
rLOX wt
rLOX mt
No. of migrated cells
1000
800
600
400
200
0
**
***
***
0 10 0 10 0 10 (μM)
Y27632
No. of migrated cells
1000
800
600
400
200
0
***
***
***
0 100 0 100 0 100 (μM)
NSC23766
No. of migrated cells
1000
800
600
400
200
0
***
***
**
0 2 0 2 0 2 (μM)
CASIN
I
Control
rLOX wt
rLOX mt
No. of invaded cells
200
150
100
50
0
**
***
*
0 10 0 10 0 10 (μM)
Y27632
No. of invaded cells
200
150
100
50
0
***
***
***
0 100 0 100 0 100 (μM)
NSC23766
No. of invaded cells
200
150
100
50
0
**
***
*
0 2 0 2 0 2 (μM)
CASIN

Figure S3. Effects of LOX Knockdown, rLOX Treatment, and Rho GTPase Inhibitor Treatment. Related to Figure 3 . (A) Western blot analysis for ectopic expression of LOX wild type (wt) and oxidase-dead mutant (mt) in LOX-depleted MDA-MB-468 cells. (B) LOX enzymatic activity in CMs from EZH2-depleted MDA-MB-468 cells expressing EZH2 wild type (wt) or methyltransferase-dead mutant (mt) was measured by using LOX activity assay kits. Error bars represent the means ± SD (n = 3); ***P<0.001 versus Control sh (ANOVA analysis). (C) Western blot showing the expression of LOX wild type (LOX wt) transfected into MCF-7 cells. (D) OCP cells were treated with CMs from control or LOX-overexpressed MCF-7 cell for 6 days and osteoclast formation was determined by TRAP staining. Scale bar, 100 μm. Error bars represent the means ± SD (n = 4); ***P<0.001 (Student's t-test). (E) For migration assays (left), OCP cells treated with CMs from MDA-MB-468 cells depleted of LOX and/or mH2A1 were seeded and incubated for 5 h in transwell inserts for migration. For invasion assays (right), MDA-MB-468 cells depleted of LOX and/or mH2A1 were seeded into upper chamber coated with Matrigel, and then allowed to invade to culture media containing 10% FBS for 48 h. The migrated and invaded cells were stained and photographed, and the number of cells that had invaded or migrated to the other pole of the membrane was counted under a light microscope. (F) Cell migration and invasion assays were performed as in (E), but LOX-depleted MDA-MB-468 cells expressing LOX wild type (wt) and mutant (mt) and their CMs were used. (G) Cell migration and invasion assays were performed as in (E), but using wild type (wt) or mutant (mt) rLOX-transfected MDA-MB-468 cells and their CMs. Error bars in (E-G) represent the means ± SD (n = 3); *P<0.05, **P<0.01, ***P<0.001 versus Control sh CM or Control (ANOVA analysis). (H) The lower side of transwell filters was coated with rLOX wt or mt in MDA-MB-468 CMs for 16 h. OCP cells were detached and seeded into the upper chamber of transwell filters, and then allowed to adhere for 1 h. Y27632 (RhoA inhibitor), NSC23766 (Rac1 inhibitor), and CASIN (Cdc42 inhibitor) were added to the lower chamber and then allowed to further migrate for 5 h. (I) MDA-MB-468 cells were detached and resuspended in culture media containing rLOX wt or mt. The suspended cells were pretreated with Y27632, NSC23766, or CASIN, seeded onto the upper chamber coated with Matrigel, and then allowed to invade for 48 h. Error bars in (H) and (I) represent the means ± SD (n = 3); *P<0.05, **P<0.01, ***P<0.001(ANOVA analysis).

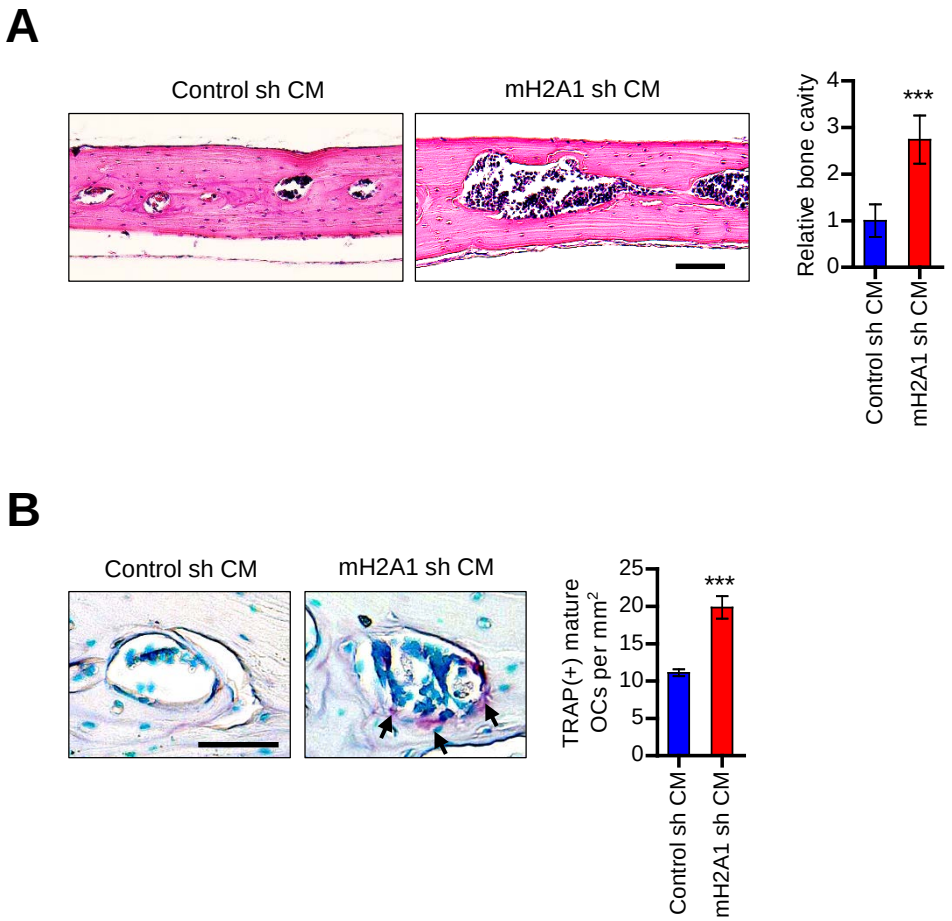

Figure S4. In Vivo Osteoclastogenic Effects of CMs Collected from mH2A1-Depleted Cells. Related to Figure 4. CMs were prepared from control shRNA or mH2A1 shRNA-infected MDA-MB-468 cells and concentrated 10-fold with a 10-kDa cut-off centrifugal filter. Calvarial bones of C57BL/6 female mice were injected with CMs (100 μl) from mock-depleted (Control sh CM) or mH2A1-depleted (mH2A1 sh CM) MDA-MB-468 cells. Calvarial bones were fixed, embedded, and stained for H&E (A) and TRAP (B). Representative images of H&E and TRAP staining are shown on the left (scale bar, 100 μm). Quantification of osteolytic legion formation and TRAP positive mature osteoclasts is shown on the right. Arrows point to TRAP+ mature osteoclasts. Error bars represent the means ± SD (n = 5); ***P<0.001 versus Control sh CM (Student's t-test).

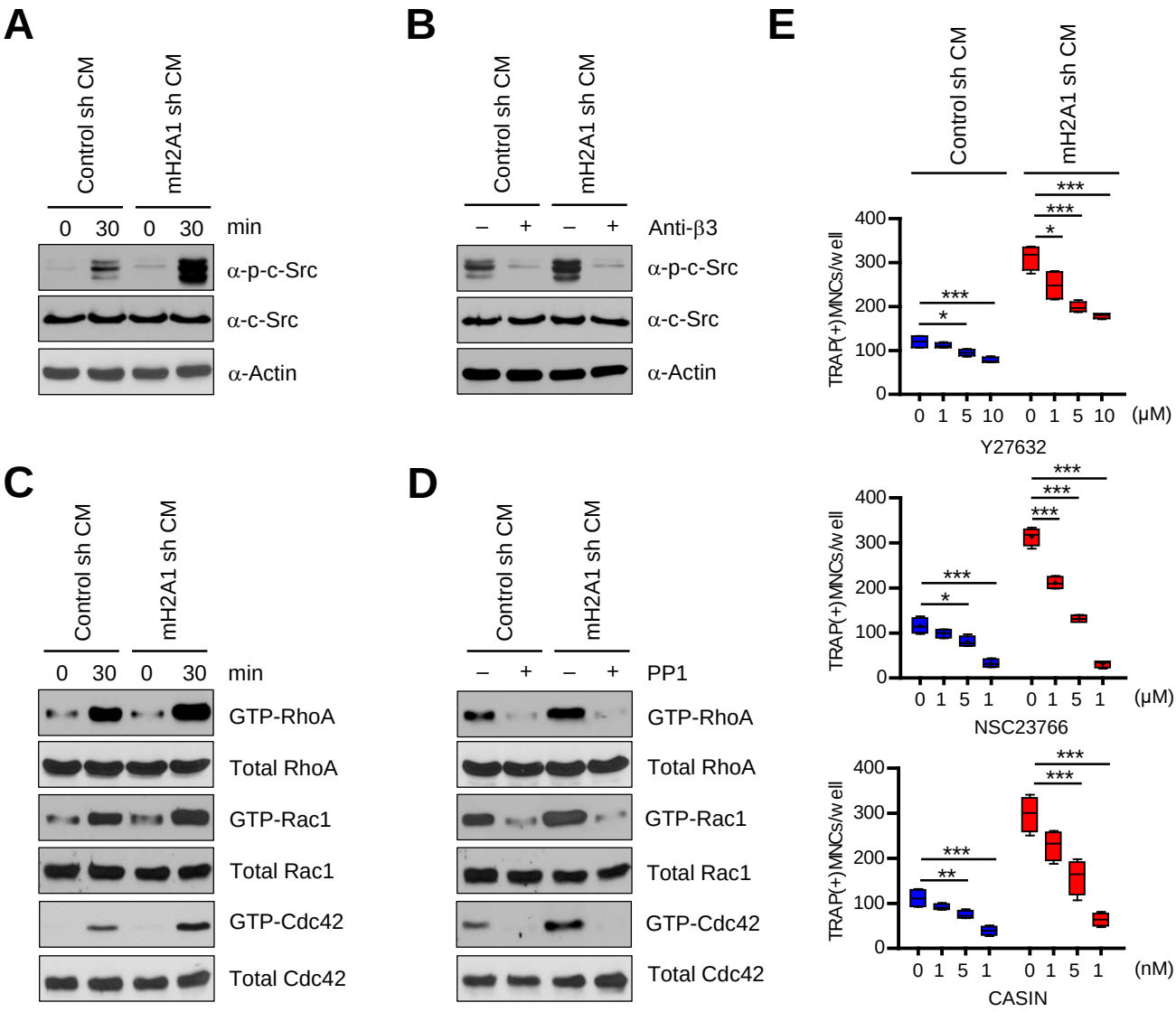

Figure S5. Effects of mH2A1-Depleted MDA-MB-468 CMs on c-Src and small GTPase Signaling. Related to Figure 5. (A) OCP cells were incubated with M-CSF (15 ng/ml) and RANKL (15 mg/ml) for 3 days and treated with CMs collected from control or mH2A1-depleted MDA-MB-468 cells for 24 h. After M-CSF/RANKL starvation for 4 h, cells were detached and resuspended in α-MEM with 0.5% FBS. The cells were seeded onto culture dishes coated with control or mH2A1-depleted MDA-MB-468 CMs and cultured for 30 min. The cells were lysed and subjected to Western blot with antibodies against c-Src and phosphorylation of c-Src. β-Actin was used as a loading control. (B) OCP cells were detached, resuspended, and pretreated with integrin β3 blocking antibody for 15 min. The cells were plated into coated with CMs from control or mH2A1-depleted MDA-MB-468 cells and incubated for 30 min. Cell lysates were then prepared and analyzed by Western blot with phospho-c-Src and c-Src antibodies. β-Actin was used as a loading control. (C) RhoA/Rac1/Cdc42 GTPases assays were done as described in Experimental Procedures, and whole cell lysates were analyzed by Western blot. (D) Small GTPases assays were performed as in (B), but using PP1 (Src inhibitor). (E) OCP cells were incubated with CMs from control or mH2A1-depleted MDA-MB-468 cells in the presence of the indicated inhibitors (RhoA inhibitor Y27632, Rac1 inhibitor NSC23766, or Cdc42 inhibitor CASIN) for 6 days. Mature osteoclasts were TRAP-stained and counted. Error bars represent the means ± SD (n = 4); *P<0.05, **P<0.01, ***P<0.001 (ANOVA analysis).

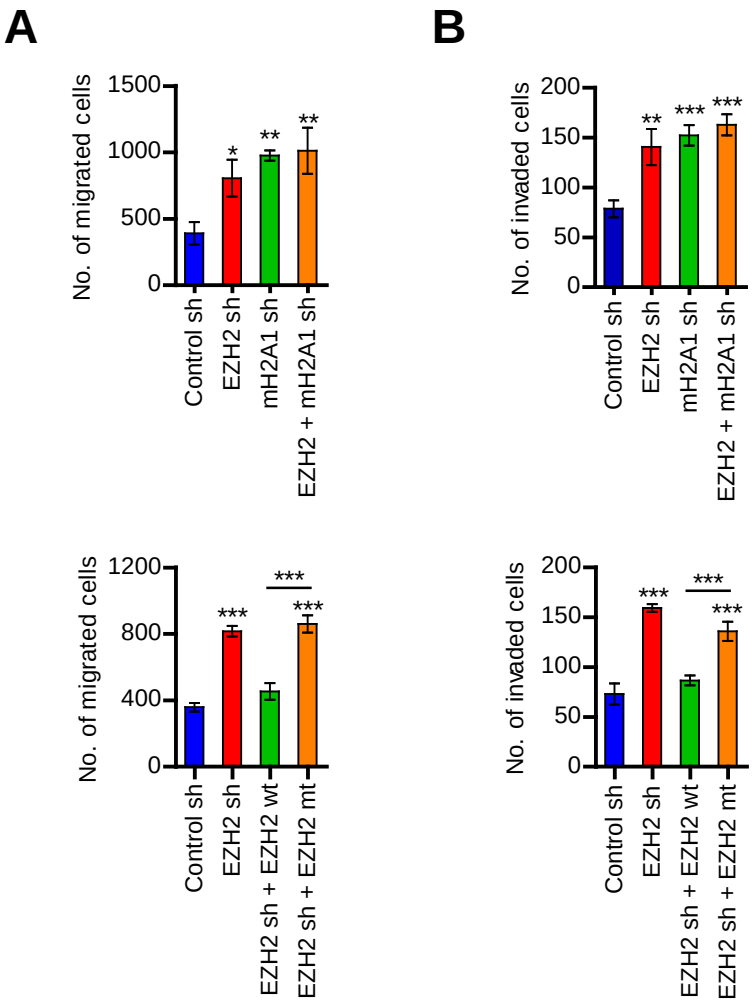

Figure S6. Effects of Soluble Factors Released by EZH2-depleted Cells on OCP Cell Migration and MDA-MB-468 Cell Invasion. Related to Figure 7. (A) OCP cells were treated with CMs from MDA-MB-468 cells depleted of EZH2 and/or mH2A1, and subjected to cell migration assays (upper). CMs from EZH2-depleted MDA-MB-468 cells expressing EZH2 wild type (wt) or enzymatically dead mutant (mt) were also used for assays (lower). (B) MDA-MB-468 cells were depleted of EZH2 and/or mH2A1 and applied to cell invasion assays (upper). Cell invasion assays were also performed with EZH2-depleted cells expressing EZH2 wt or mt (lower). Error bars in (A) and (B) represent the means ± SD (n = 3); *P<0.05, **P<0.01, ***P<0.001 versus Control sh CM (ANOVA analysis).

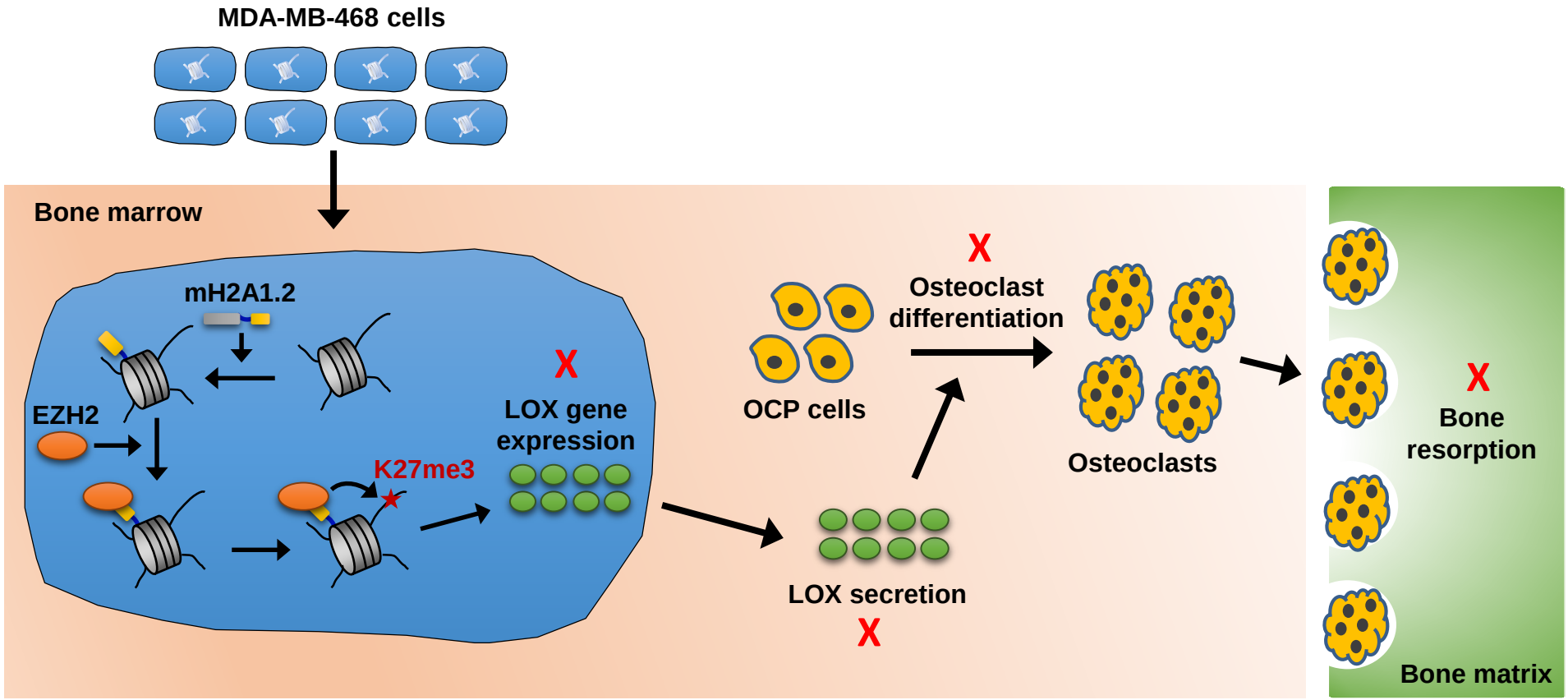

Figure S7. Model for the Cooperative Role of mH2A1.2 and EZH2-Mediated H3K27me3 in Regulating LOX Expression and Osteoclastogenesis. Related to Figure 1-7. See DISCUSSION for more details.

SUPPLEMENTAL EXPERIMENTAL PROCEDURES

RNAi, ChIP, and qRT-PCR

DNA oligonucleotides encoding shRNAs specific for the 3'UTR or CDS regions of histone variants, LOX and EZH2 (listed in Table S1) were subcloned into pLKO.1 lentiviral expression vector (Addgene) according to standard procedures (https://www.addgene.org/tools/protocols/plko/). Lentiviral particles were generated in 293T cells by co-transfecting plasmids encoding VSV-G, NL-BH and the shRNAs. MDA-MB-468 breast cancer cells were infected with these viruses and selected with puromycin (2 μg/ml) for two weeks. ChIP assays were performed using mH2A1 and EZH2 antibodies and the ChIP assay kit (Millipore) as previously described (Kim et al., 2016b). DNA molecules immunoprecipitated from MDA-MB-468 cells were analyzed by qPCR using the primers that amplify the five different regions extending over 8 kb including approximately 4 kb upstream and 4 kb downstream of transcription start sites of the *LOX*, *GAS6*, *NOV*, *IL1B*, *BMP4*, and *TRPC1* genes. The primers used for qPCR are listed in Table S4. All qPCR reactions were run in triplicate, and specificity of amplification was determined by melting curve analysis. For qRT-PCR, total RNA was isolated from MDA-MB-468 cells using an RNeasy mini kit (Qiagen). After converting RNA to cDNA using iScript cDNA Synthesis Kit (Bio-Rad), real-time RT-PCR was performed using one-step QuantiTect SYBR Green RT-PCR kit (Qiagen) according to the manufacturer's instructions. The primers used quantitative real-time PCR are listed in the Table S4.

Constructs and Antibodies

Bacterial expression constructs of mH2A1.2 and EZH2 were generated by PCR-amplifying and sub-cloning their cDNAs into pGEX-4T1 and pET15b vectors. For mammalian expression of H2A, mH2A1.1, mH2A1.2, LOX and EZH2, the corresponding cDNAs were amplified by PCR and ligated into the correct reading frames of lentiviral expression vector pLenti-Hygro (Addgene) containing 5' FLAG coding sequences. To prepare lentiviral particles for H2A, mH2A1.1, mH2A1.2, LOX and EZH2, 293T cells were transfected with plasmids encoding VSV-G, NL-BH and the pLenti-Hygro constructs (H2A, mH2A1.1, mH2A1.2, LOX and EZH2) using Lipofectamine 2000 (Invitrogen). MDA-MB-468 breast cancer cells stably expressing the pLenti-Hygro constructs were generated by lentivirus infection and subsequent selection for Hygromycin B (200 μg/ml, Invitrogen) resistance for two weeks. To generate shRNA-resistant mH2A1.1 and mH2A1.2 expression vectors, wild type mH2A1.1 and mH2A1.2 constructs were point-mutated by the QuikChange® II site-directed mutagenesis kit according to manufacturer's protocol (Agilent Technologies). Further details of plasmid constructions are available upon request. The following antibodies were used in this study: Cathepsin K (cat.no. ab19027), H3

(cat.no. ab1791), H3K4me1 (cat.no. ab176877), H3K4me3 (cat.no. ab8580), H3K36me1 (cat.no. ab9048), and H3K36me3 (cat.no. ab9050) antibodies from Abcam, β-Actin (cat.no. A5441), FLAG (cat.no. F1804), and HA (cat.no. H3663) antibodies from Sigma-Aldrich, His (cat.no. LT0426) antibody from Lifetein, EZH2 (cat.no. 39901), H3ac (cat.no. 61637), H4ac (cat.no. 39925), H3K9me3 (cat.no. 39161), and H3K27me1 (cat.no. 61015) antibodies from Active Motif, ATP6V0D2 (cat.no. sc-69111), c-Src (cat.no. sc-19), GST (cat.no. sc-138), and NFATc1 (cat.no. sc-13033) antibodies from Santa Cruz Biotechnology, Cdc42 (cat.no. 240201), RhoA (cat.no. 240302), and Rac1 (cat.no. 240106) antibodies from Cell Biolabs, p-c-Src (Tyr416) (cat.no. 2101) antibody from Cell Signaling, and H2Aac (cat.no. 07-376), H2Bac (cat.no. 07-373), H3K4me2 (cat.no. 07-030), H3K9me1 (cat.no. 07-450), H3K9me2 (cat.no. 07-441), H3K27me2 (cat.no. 07-452), H3K27me3 (cat.no. 07-449), H3K36me2 (cat.no. 07-369), Integrin β3 (cat.no. MAB2023Z) and LOX (cat.no. ABT112) antibodies from Millipore.

Generation of Breast Cancer Secretome

To generate a breast cancer secretome, we used the secretory protein accession numbers from the expressed genes from various databases as well as published studies as summarized in Supplementary Table S2. Within each secretome source database, only human specific proteins were searched. Protein IDs or hugo gene names were interconverted to unique gene IDs using BiodBnet (https://biodbnet-abcc.ncifcrf.gov/) and DAVID (http://david.abcc.ncifcrf.gov/conversion.jsp). A subset of proteins with a predicted signal peptide and experimentally confirmed to be secretory or localized in membrane were created. All identified secretory proteins were mapped to genes corresponding to GRCh37. Mapping of these identified proteins on Illumina transcriptome Human HT-12 V4 expression ChIP identified a subset of 6,267 candidate probes, which represents ‘secretome array’ of breast in the present study. To avoid any redundancy, further analysis was performed with the 6,267 probes (or 3948 genes) including genes encoding breast specific secretory proteins.

Tissue qPCR Array

TissueScan Breast Cancer and Normal Tissue cDNA array (BCRT102/302/502) was obtained from Origene Technologies. The array contained a panel of dried cDNAs from 48 samples including five normal samples. The expression of mH2A1.2 and LOX was measured by using SYBR Green PCR kit (Qiagen). A description in depth pathology report (including histology sections) for all of the RNA molecules used in the panel can be viewed in Table S5 and OriGene’s Website.

Cell Migration and Invasion Assay

For migration assays, the lower side of transwell filters was coated with rLOX wt (100 ng/ml) or LOX mt (100 ng/ml) in the presence of MDA-MB-468 CMs for 16 h and then blocked with 1% BSA for 1 h. OCP cells (1×10^5 cells) were seeded onto the upper chamber of transwell filters in α-MEM containing 0.5% FBS. After rLOX wt or rLOX mt were added to the lower chamber in α-MEM culture medium containing M-CSF (15 ng/ml) and RANKL (15 ng/ml), cells were allowed to migrate to lower chamber for 5 h. For invasion assays, the transwell filters were coated with Matrigel (BD Biosciences) for 1h. MDA-MB-468 cells (1×10^5 cells) were detached and resuspended in DMEM containing 0.5% FBS, rLOX wt (100 ng/ml), or rLOX mt (100 ng/ml), and then seeded onto the upper chamber of transwell filers. The culture media in the lower chamber contained 10% FBS, rLOX wt or rLOX mt. The cells were allowed to invade for 48 h. The invaded or migrated cells were fixed with 3.7% formalin for 15 min, stained with 1% crystal violet for 1 h, and photographed. For each experiment, pictures of 5 fields (equal size) were taken and the cells have been counted.

LOX Enzyme Activity Assay

LOX activity in the conditioned media (50 μl) was measured by using a LOX activity assay kit according to manufacturer's instructions (Abcam). Samples were placed on ice and changes in fluorescence were measured using a fluorescence spectrophotometer with excitation and emission wavelengths 540 and 590 nm respectively. The level of hydrogen peroxide generated by LOX enzymatic activity was determined by comparing fluorescence changes to a standard plot, relating fluorescence change to nmoles of hydrogen peroxide added to assays lacking LOX. The value corresponding to the amount of hydrogen peroxide produced was then normalized to total protein.

RhoA/Rac1/Cdc42 GTPase and Western Blot Analysis

The assays for measuring RhoA, Rac1, and Cdc42 GTPase activities were performed using RhoA/Rac1 assay kit according to manufacturer's protocol (Cell Biolabs). OCP cells were lysed with a lysis buffer (50 mM Tris-HCl, pH 7.5, 10 mM $MgCl_2$, 150 mM NaCl, 2% NP40, and 1x Roche protease inhibitor cocktail). After centrifuging cell lysates, the supernatants were incubated with Rhotekin RBD agarose (Cell Biolabs) or PAK1 PBD agarose (Cell Biolabs) for 2 h. The mixture was washed, re-suspended in lysis buffer, and applied to Western blotting. For Western blot analysis of c-Src and small GTPases (RhoA, Rac and Cdc42), OCP cells (1×10^6/100-mm culture dish) were incubated with M-CSF (15 ng/ml) and RANKL (15 ng/ml) for 3 days and treated with rLOX (100 ng/ml) in 10% FBS for 24 h. After 4 h starvation of M-CSF, RANKL and rLOX in α-MEM medium, cells were transferred to culture dishes

coated with rLOX in MDA-MB-468 CMs and cultured at 37°C over a 30-min time period. The cells were then lysed and subjected to Western blot analysis.

Bone Resorption Assay

Osteoclasts were plated on dentin slices (IDS Ltd.), treated with rLOX wt or rLOX mt (100 ng/ml) in MDA-MB-468 CMs containing M-CSF (30 ng/ml) and RANKL (30 ng/ml), and further cultured for 48 h to resorb bone. Dentine slices were then ultrasonicated to remove adherent cells, and resorption pits on the slice were stained with 1% toluidine blue. The resorbed area was analyzed using Image-Pro Plus program (MediaCybernetics).

cDNA Microarray Analysis

Total RNA was extracted from mock- or mH2A1-depleted MDA-MB-468 cells using the TRI-zol reagent (Invitrogen), and hybridized on whole-genome expression array (Human HT-12 v4 Expression BeadChip, Illumina). To detect differential expression of genes corresponding to secreted factors, microarray data were background corrected with GenomeStudio based on manufacturer's recommendation and normalized using limma package (Ritchie, et al., 2015). Probe level data were summarized into a single expression value for each gene, and were further analyzed with 3948 candidate virtual secretome genes. Differences in mRNA levels between control and mH2A1-depleted cells were determined using strict statistical criteria of detection p-value in all replicates $p<0.05$. The gene expression array data have been deposited in the NCBI Gene Expression Omnibus (GEO) database under the GEO accession number GSE107570.

Pathway-Based Approach for Secretory Biomarker Discovery and Candidate Gene Prioritization

To study the potential functional significance of all secretome genes, we quarried different signature databases such as Gene ontology, Mammalian phenotype, Pathway, Protein domain, PubMed, Protein Interaction, and Gene Expression. Hypergeometric distribution along with Benjamini Hochberg correction was used as the standard method for determining p value of significance. Further, fisher's inverse chi-square method was used to combine p-values from multiple features/annotations into an overall P-value to rank the genes with each pathway ($p<0.05$). A functional annotation-based candidate gene prioritization approach based on a fuzzy-based similarity between two genes in semantic annotations was used as described previously (Kaimal et al., 2011; Punj et al., 2012). This approach uses a protein interaction database derived from the entire Medline abstract database. Such analysis was aimed to explore the global and systemic properties of the biomarker underlying molecular networks of the

biomarker and enables interpretation of the biologic significance of the gene list. This annotation was used to prioritize candidate biomarkers for validation.

Purification and Analysis of Nucleosomes

Nuclear pellets were prepared from MDA-MB-468 cells transfected with FLAG-tagged H2A and mH2A1.2, and were digested with micrococcal nuclease in nuclear extraction buffer (20 mM HEPES, pH 7.4, 500 mM NaCl, 1.5 mM $MgCl_2$, 0.2 mM EGTA, and 1x Roche protease inhibitor cocktail) to produce predominantly mononucleosomes. After adjusting the salt concentration of the reaction to 300 mM NaCl, ectopic H2A/mH2A1.2-containing nucleosomes were purified by immunoprecipitation on anti-FLAG antibody-conjugated agarose beads in washing buffer (20 mM HEPES, pH 7.8, 300 mM NaCl, 1.5 mM $MgCl_2$, 0.2 mM EGTA, 10% Glycerol, 0.2% Triton X-100, and 1x Roche protease inhibitor cocktail). Bead-bound nucleosomes were analyzed by Western blot using antibodies against specific histone modifications.

Protein-Protein Interaction

GST and GST-tagged proteins were expressed in E. coli Rosetta 2 (DE3) pLysS (Novagen) and purified on Glutathione-Agarose beads (Sigma-Aldrich) as described previously (Kim et al., 2015). In vitro binding assays were performed with equal amounts of GST or GST fusion proteins in affinity buffer (20 mM HEPES-KOH, pH 7.9, 0.5 mM EDTA, 200 mM NaCl, 10% glycerol, and 0.1% Nonidet P-40) supplemented with PMSF, DTT, and protease inhibitor mixture. Bound proteins were washed four times with affinity buffer, and detected by Western blotting. Ten percent of the interaction mix were loaded as an input fraction.

Co-Immunoprecipitation

MDA-MB-468 breast cancer cells were lysed in cell lysis buffer (50 mM Tris-HCl, pH 7.4, 150 mM NaCl, 1 mM EDTA, and 1% Triton X-100) supplemented 1x Roche protease inhibitor cocktail. Cell lysate materials were pre-cleared for 1 h with A/G beads (Santa Cruz Biotechnology) and then incubated with mH2A1 and EZH2 antibodies overnight. As a negative control, normal IgG was used that showed negligible signal. The following day, A/G agarose beads were added to the immunoprecipitates for 1 h. After washing the beads four times with lysis buffer, the binding of endogenous mH2A1 and EZH2 was examined by Western blot.

Statistical Analysis

All quantitative data are presented as mean ± SD. Statistical analyses of datasets were performed with Student's two-tailed *t*-test or two-way ANOVA followed by Bonferroni's comparison test. GraphPad Prism (GraphPad Software Inc.) was used for all analyses. A P value < 0.05 was considered statistically significant.

SUPPLEMENTAL REFERENCES

Kaimal, V., Sardana, D., Bardes, E.E., Gudivada, R.C., Chen, J. and Jegga, A.G. (2011) Integrative systems biology approaches to identify and prioritize disease and drug candidate genes. Methods. Mol. Biol. *700*, 241-259.

Kim, H., Heo, K., Choi, J., Kim, K. and An, W. (2011). Histone variant H3.3 stimulates HSP70 transcription through cooperation with HP1gamma. Nucleic Acids Res. *39*, 8329-8341.

Kim, J.M., Heo, K., Choi, J., Kim, K. and An, W. (2013a). The histone variant MacroH2A regulates Ca(2+) influx through TRPC3 and TRPC6 channels. Oncogenesis *2*, e77.

Kim, J.M., Kim, K., Punj, V., Liang, G., Ulmer, T.S., Lu, W. and An, W. (2015). Linker histone H1.2 establishes chromatin compaction and gene silencing through recognition of H3K27me3. Sci Rep *5*, 16714.

Kim, J.M., Kim, K., Schmidt, T., Punj, V., Tucker, H., Rice, J.C., Ulmer, T.S. and An, W. (2015) Cooperation between SMYD3 and PC4 drives a distinct transcriptional program in cancer cells. Nucleic Acids Res. *43*, 8868-8883.

Kim, K., Punj, V., Choi, J., Heo, K., Kim, J.M., Laird, P.W. and An, W. (2013b). Gene dysregulation by histone variant H2A.Z in bladder cancer. Epigenetics Chromatin *6*, 34.

Kim, K., Punj, V., Kim, J.M., Lee, S., Ulmer, T.S., Lu, W., Rice, J.C. and An, W. (2016b). MMP-9 facilitates selective proteolysis of the histone H3 tail at genes necessary for proficient osteoclastogenesis. Genes Dev 30, 208-219.

Punj, V., Matta, H. and Chaudhary, P.M. (2012) A computational profiling of changes in gene expression and transcription factors induced by vFLIP K13 in primary effusion lymphoma. PLoS One *7*, e37498.

Ritchie, M.E., Phipson, B., Wu, D., Hu, Y., Law, C.W., Shi, W. and Smyth, G.K. (2015) limma powers differential expression analyses for RNA-sequencing and microarray studies. Nucleic Acids Res. *43*, e47.